### Title

Riluzole and novel naphthalenyl substituted aminothiazole derivatives prevent acute neural excitotoxic injury in a rat model of temporal lobe epilepsy




### Authors

Kyllo, Thomas
Singh, Vikrant
Shim, Heesung
et al.



### Publication Date

2023-02-01

### DOI

10.1016/j.neuropharm.2022.109349

Peer reviewed

HHS Public Access

Author manuscript

*Neuropharmacology*. Author manuscript; available in PMC 2023 February 15.

Published in final edited form as:

*Neuropharmacology*. 2023 February 15; 224: 109349. doi:10.1016/j.neuropharm.2022.109349.

# Riluzole and novel naphthalenyl substituted aminothiazole derivatives prevent acute neural excitotoxic injury in a rat model of temporal lobe epilepsy

**Thomas Kyllo**[a,1], **Vikrant Singh**[b,1], **Heesung Shim**[b], **Singh Latika**[b], **Hai M. Nguyen**[b], **Yi-Je Chen**[b], **Ellen Terry**[a], **Heike Wulff**[b], **Jeffrey D. Erickson**[a,*]

[a]Neuroscience Center of Excellence, School of Medicine, Louisiana State University Health-New Orleans, New Orleans, LA, USA

[b]Department of Pharmacology, School of Medicine, University of California-Davis, Davis, CA, USA

## Abstract

Epileptogenic seizures, or status epilepticus (SE), leads to excitotoxic injury in hippocampal and limbic neurons in the kainic acid (KA) animal model of temporal lobe epilepsy (TLE). Here, we have further characterized neural activity regulated methylaminoisobutryic acid (MeAIB)/glutamine transport activity in mature rat hippocampal neurons *in vitro* that is inhibited by riluzole ($IC_{50}$ = 1 μM), an anti-convulsant benzothiazole agent. We screened a library of riluzole derivatives and identified SKA-41 followed by a second screen and synthesized several novel chlorinated aminothiazoles (SKA-377, SKA-378, SKA-379) that are also potent MeAIB transport inhibitors *in vitro*, and brain penetrant following systemic administration. When administered before KA, SKA-378 did not prevent seizures but still protected the hippocampus and several other limbic areas against SE-induced neurodegeneration at 3d. When SKA-377 - 379, (30 mg/kg) were administered after KA-induced SE, acute neural injury in the CA3, CA1 and CA4/hilus was also largely attenuated. Riluzole (10 mg/kg) blocks acute neural injury. Kinetic analysis of SKA-378 and riluzoles' blockade of $Ca^{2+}$-regulated MeAIB transport in neurons *in vitro* indicates that inhibition occurs *via* a non-competitive, indirect mechanism. Sodium channel $Na_V1.6$ antagonism blocks neural activity regulated MeAIB/Gln transport *in vitro* ($IC_{50}$ = 60 nM)



*Corresponding author. jerick@lsuhsc.edu (J.D. Erickson).

[1]T.K. and V.S. contributed equally to this work.

CRediT authorship contribution statement

**Thomas Kyllo:** Investigation, Data curation, Methodology, Validation, Visualization, Formal analysis, Writing – review & editing. **Vikrant Singh:** Investigation, Resources, Data curation, Methodology, Formal analysis, Validation. **Heesung Shim:** Investigation, Data curation, Resources. **Singh Latika:** Investigation, Data curation, Resources. **Hai M. Nguyen:** Investigation, Formal analysis. **Yi-Je Chen:** Investigation. **Ellen Terry:** Investigation. **Heike Wulff:** Conceptualization, Methodology, Validation, Formal analysis, Resources, Writing – review & editing, Visualization, Supervision, Project administration. **Jeffrey D. Erickson:** Conceptualization, Methodology, Validation, Formal analysis, Investigation, Writing – original draft, Writing – review & editing, Visualization, Supervision, Project administration, Funding acquisition.

Declaration of competing interest

The authors have no conflict of interests.

Appendix A. Supplementary data

Supplementary data to this article can be found online at https://doi.org/10.1016/j.neuropharm.2022.109349.

and SKA-378 is the most potent inhibitor of $Na_V1.6$ ($IC_{50}$ = 28 μM) compared to $Na_V1.2$ ($IC_{50}$ = 118 μM) in heterologous cells. However, pharmacokinetic analysis suggests that sodium channel blockade may not be the predominant mechanism of neuroprotection here. Riluzole and our novel aminothiazoles are agents that attenuate acute neural hippocampal injury following KA-induced SE and may help to understand mechanisms involved in the progression of epileptic disease.

**Keywords**

Glutamate/glutamine cycle; Kainic acid/excitotoxin; Neuroprotection/neurodegeneration; Temporal lobe epilepsy/epileptic disease; Status epilepticus/epileptogenic seizure; Riluzole/benzothiazole/aminothiazole/antiepileptic drugs

## 1. Introduction

Temporal lobe epilepsy (TLE) is a common and debilitating chronic neurologic disorder (Sirven, 2015; Devinsky et al., 2018). Currently, most antiseizure drugs (ASDs) used in the treatment of epilepsy are prescribed to prevent recurrent epileptic seizure activity and target mechanisms that increase inhibitory GABA transmission or reduce Glu excitatory transmission (Meldrum and Rogawski, 2007; Sills and Rogawski, 2020). Glu is the major excitatory neurotransmitter in the brain and is also a potent excitotoxin that after excessive synaptic release during seizure activity can lead to both acute and chronic neural injury (Holmes, 2002; Dudek and Sutula, 2007; Bittigau and Ikonomidou, 1997; Dodd, 2002; Rothstein et al., 1996). Here, we utilized the KA rat model of TLE to produce limbic seizures and hippocampal neural injury consistent with that seen in humans (Ben Ari, 1985; Sperk, 1994; Sharma et al., 2007; Levesque, 2013; Rusina et al., 2021). KA is a potent Glu excitotoxin that stimulates excessive presynaptic Glu release from dentate gyrus (DG) mossy fibers onto excitatory CA3 pyramidal neurons and mossy cells in the hilar region. Glu-induced excitotoxicity then proceeds to CA3-CA1 collateral subfields within the hippocampus and then *via* inter-connected excitatory hippocampal output projections to other limbic areas of the brain producing neural injury in multiple regions (Nadler, 1981; Ferkany and Coyle, 1983; Henze et al., 2000; Hopkins et al., 2000; Wang et al., 2005; Srivastava et al., 2020). The process of epileptogenesis is not clearly understood, but in the KA model of TLE it is initiated by epileptogenic seizures (Dudek and Sutula, 2007; Ben Ari, 1985; Sperk, 1994; Sharma et al., 2007; Levesque, 2013; Rusina et al., 2021; Wang et al., 2005), or status epilepticus (SE), as defined by stage 5 grade seizure activity using the Racine scale (Racine, 1972). SE results in acute hippocampal neural injury in the KA model of TLE and then during a ‘silent period’ (3–6 months) leads to hippocampal sclerosis and alterations in neuronal circuitry that eventually leads to spontaneous recurrent epileptic seizures (Bouilleret et al., 1999; Riban et al., 2002; Dunleavy et al., 2010), which most clinicians would define as epilepsy (Fisher et al., 1998; Watson, 2003; Janszky et al., 2005; Blumcke et al., 2012; Thom, 2014). Late-stage drug-resistant TLE results from the inability of ASD’s to prevent recurrent epileptic seizure activity (Tang et al., 2017; Loscher et al., 2020). In addition, many of the ASD’s used today have consequential negative side effects such as sedation, mental slowing, and motor reflex reduction (Walia et al., 2004; Perucca and Gilliam, 2012; Thigpen et al., 2013). A critical goal going forward is to identify new

synaptic targets and to develop antiepileptic drugs (AEDs) specific to these targets to prevent acute hippocampal neural injury that can lead to epileptogenesis and epileptic disease, which would be most beneficial in clinical settings (White and Bialer, 2010; Loscher and Schmidt, 2011; Kaminski et al., 2014; Loscher, 2020; Benassi et al., 2021; Marques et al., 2022).

Riluzole is an anti-glutamatergic neuroprotective agent in several animal models of neural injury (Doble, 1996; Stutzmann et al., 1997) and is thought to act by reducing synaptic Glu release from axonal synapses (Martin et al., 1993; Lingamaneni and Hemmings, 1999; Wang et al., 2004), and thus excitotoxicity. Riluzole, also called Rilutek®, is an FDA approved drug for amyotrophic lateral sclerosis (ALS) (Salameh et al., 2015). Even though riluzole and other similar benzothiazole derivatives are also anti-convulsant agents (Mizoule et al., 1985; Romettino et al., 1991; Jimonet et al., 1994; Borowicz et al., 2004; Kim et al., 2007; Ugale et al., 2012; Ali and Siddiqui, 2013; Coleman et al., 2015; Jagbir et al., 2015), they are not utilized in epilepsy therapy in Europe or the United States. Riluzole's ability to inhibit various activities varies with potency *in vitro* (μM - mM) among its multiple targets throughout the brain and spinal cord. Riluzole's neuroprotective actions may include the inhibition of $Na^+$ channel activity (Herbert et al., 1994; Song et al., 1997; Stefani et al., 1997; Prakriya and Mennerick, 2000; Spadoni et al., 2002); $K^+$ and $Ca^{2+}$ channel activity (Zona et al., 1998; Grunnet et al., 2001; Duprat et al., 2000; Huang et al., 1997), protein kinase activity (Noh et al., 2000), and Glu receptor activity (Debono et al., 1993; Zona et al., 2002). Riluzole has also been reported to stimulate small-conductance $Ca^{2+}$-activated $K^+$ channels (Sankaranarayanan et al., 2009) and the activity of synaptic Glu clearance transporters (Fumagalli et al., 2008) located on perisynaptic astrocytes that are critically important to resist direct Glu excitotoxicity (Sheldon and Robinson, 2007). The most potent target of riluzole is inhibition of spontaneous neuron specific, activity regulated, high affinity MeAIB/Gln transport activity in mature hippocampal neurons *in vitro* with an $IC_{50}$ ~1 μM (Erickson, 2017). Based on these multiple pharmacological activities, riluzole constitutes what has been termed a 'privileged structure', meaning a small, typically bicyclic ring system that is known to exert multiple biological activities and therefore can serve as a template for the design of drugs to inhibit or activate one of these targets selectively by appropriately decorating it with substituents (Horton et al., 2003; Priyanka and Jha, 2010; Sharma et al., 2012).

MeAIB is considered a selective substrate for a low affinity ($K_m$ ~ 0.5 mM) neutral amino acid transport system originally defined as system A in mostly all cells, which prefers alanine described years ago (Christensen, 1990). System A transporters in the SLC38 gene family are called SNATs, which translates to Sodium-coupled Neutral Amino Acid Transporters or System N and A Transporters (Mackenzie and Erickson, 2004). SNAT1 and SNAT2 are the major $Na^+$-coupled neutral amino acid transporters expressed in neurons (Varoqui et al., 2000; Yao et al., 2000; Reimer et al., 2000; Chaudhry et al., 2002a). Gln is a substrate of system A and the most abundant neutral amino acid in cerebral spinal fluid (CSF) (Gjessing et al., 1972; McGale et al., 1977). SNATs have been proposed to be a critical conduit from glia to provide Gln as precursor to neurotransmitter Glu synthesis and $Ca^{2+}$-dependent Glu release from neuronal synapses (Mackenzie and Erickson, 2004; Chaudhry et al., 2002b), but *see* (Conti and Melone, 2006). Once released from axon terminals Glu is cleared from the synaptic cleft by Glu transporters on astrocytes (Danbolt,

2001), converted to Gln by Gln synthetase (Norenberg and Martinez-Hernandez, 1979), released from astrocytes (Deitmer et al., 2003; Leke and Schousboe, 2016), imported to axon terminals by unknown mechanisms, and then converted to Glu *via* phosphate-activated glutaminase (Kvamme et al., 2001; Masson et al., 2006) for exocytotic release. Replenishment and maintenance of cytoplasmic Glu levels in axon terminals by Glu/Gln cycling may be required for continued Glu synaptic release under prolonged $Ca^{2+}$-regulated excitotoxic conditions (Marx et al., 2015; Pietrancosta et al., 2020), but *see* (Kam and Nicoll, 2007). Other metabolic pathways to neurotransmitter Glu synthesis and release have also been postulated (Schousboe et al., 1997; Hassel and Brathe, 2000; Takeda et al., 2012). Models of epilepsy in rodents support a role for MeAIB/Gln transport *via* the Gln-Glu cycle to sustain seizure activity because Glu-induced epileptiform activity is reduced in neurons by application of MeAIB *in vitro* and *in vivo* (Bacci et al., 2002; Tani et al., 2007, 2010, 2014; Kanamori and Ross, 2013).

Here, we screened two riluzole based libraries (Sankaranarayanan et al., 2009; Shim et al., 2019) to identify compounds that possess the ability to inhibit spontaneous neural activity regulated, high affinity MeAIB/Gln transport in hippocampal neurons *in vitro* as potently as riluzole (Erickson, 2017), but are structurally unique. Based upon these screens, we have synthesized several novel chlorinated naphthalenyl substituted aminothiazoles that also potently inhibit activity regulated MeAIB/Gln transport activity at the plasma membrane in mature hippocampal neurons *in vitro*. The original compound identified in our first screen (SKA-41) and our most potent chlorinated derivatives *in vitro* (SKA-378, SKA-377 and SKA-379) exhibit excellent ‘drug-like’ properties with high oral availability and good brain penetration. We therefore tested riluzole and several of these novel aminothiazole derivatives in the KA-model of TLE.

The ability to prevent epileptic disease associated with TLE may depend on the ability of drugs to limit acute and subsequent chronic hippocampal neural injury following epileptogenic seizures. The neuroprotective effect of riluzole in the KA model of TLE has not previously been examined. We are the first to administer riluzole after SE in the literature; in this case, 1 h after the first KA-induced SE event. Our results demonstrate that riluzole, SKA-378 and SKA-379 are the most neuroprotective agents described when measured after 3 d in this acute model of KA neural injury. Riluzole and our novel aminothiazole derivatives of riluzole may be useful tools to further understand the mechanisms that prevent neural injury in the hippocampus and associated limbic regions following KA-induced SE that may lead to the progression of TLE. In addition, riluzole, SKA-378 and SKA-379 could have therapeutic value as AEDs for a potential new target.

## 2. Methods

### 2.1. Animals

We used Sprague-Dawley albino rats (Envigo, Indianapolis, IN or Charles Rivers, Wilmington, MA) for these studies. Primary hippocampal neuronal cultures were prepared from fetuses of both sexes on embryonic day 19 (E19) female rats. Adult (nine-to 11-week old, ~225 g) male rats were allowed to acclimatize to the new vivarium for 4–7 days and used for all pharmacokinetic, behavioral and *in vivo* experiments. All animal procedures

were approved by the Institutional Animal Care and Use Committee at LSUHSC and UC Davis and complied with the NIH guidelines. All measures were taken to minimize pain, discomfort, or suffering of animals and were limited to that which is unavoidable in the context of scientifically sound research. Rats were housed 2 per cage in an environmentally controlled room (23 °C, 12-h light/12-h dark cycle) with food and water available *ad libitum*. Following KA administration rats were monitored daily by us and the Division of Animal Care staff.

## 2.2. Compounds

**2.2.1. Library 1—**The commercial sourcing or the synthesis of our first screening library consisting of compounds SKA-1 to SKA-56 was described previously (Sankaranarayanan et al., 2009). All compounds were stored as dry powder at RT and were checked for potential degradation by thin layer chromatography before shipping to New Orleans.

**2.2.2. Library 2—**The syntheses of the naphthalenyl substituted aminothiazoles SKA-190, SKA-193, SKA-198, SKA-219, SKA-220, SKA-230, SKA-232, SKA-247, SKA-251, SKA-255, SKA-257, SKA-260, SKA-265, and SKA-268 were described previously (Shim et al., 2019). SKA-77 (CAS no. 77815-14-6), SKA-88 (CAS no. 1826-16-0), SKA-89 (CAS no. 19968-59-3) and SKA-94 (CAS no. 28989-50.6) were purchased from Alfa Aesar. SKA-78 (CAS no. 2010-06-2) was purchased from Acros Organics. SKA-79 (CAS no. 2103-91-5), SKA-80 (CAS no. 2103-99-3), SKA-82 (CAS no. 30709-67-2) and SKA-232 (CAS no. 2834-79-9) were purchased from Sigma-Aldrich. SKA-255 (CAS no. 438233-93-3) was purchased from Oakwood Chemical. Scaled-up synthetic procedures for resynthesis or in-house synthesis of several compounds, which were used in larger quantities, are described in the Supplemental Data.

## 2.3. New chemical synthesis

The synthesis of several active novel chlorinated (SKA-377, SKA-378, SKA-379) or brominated (SKA-375) compounds, inactive/weakly-active (SKA-262, SKA-376) or fluorinated (SKA-382) compounds derived from SKA-75 and SKA-76 is described in detail in the Supplemental Data section.

## 2.4. Cell culture

Primary hippocampal neurons were prepared from embryonic day 19 Sprague Dawley rats of both sexes as described (Erickson, 2017; Brewer et al., 1993) with minor modifications. Pregnant dams were subjected to an overdose of compressed $CO_2$ administered in an anesthesia chamber and then decapitated using a guillotine. During dissection, the hippocampi were collected in Hanks Balanced Salt Solution (without $Ca^{2+}$) containing 10 mM $MgCl_2$, 10 mM HEPES (pH 7.2), 0.2 mM Gln, penicillin (100 U/ml) and streptomycin (100 mg/ml) (pen/strep) at 4 °C. Hippocampi were then incubated in oxygenated Neurobasal medium (NB) without B27 (Invitrogen, Gaithersburg, MD) containing 0.25 mg/ml papain (Sigma, St. Louis, MO) and 0.25 mg/ml cysteine for 18 min at 37 °C with shaking. The tissue was transferred to a 15 ml conical tube containing DMEM plus 10% (v/v) fetal bovine serum (FBS) and allowed to settle. The medium was removed and the tissue was dissociated in same medium (~1 ml) by trituration with fire-polished Pasteur pipettes, the

cells were counted, diluted in DMEM containing 10% (v/v) FBS, 0.5 mM glutamax, and 25 μM Glu, and then seeded in six-well dishes (~$3 \times 10^5$ cells/well) precoated with 25 μg/ml poly-D-lysine (>300,000 MW, Sigma). After 2 h at 37 °C the medium was removed and replaced with NB medium supplemented with B27, 1% (v/v) FBS, 0.5 mM glutamax, 25 μM Glu, and pen/strep. Neurons were fed by addition of 1 ml of NB medium supplemented with B27, 0.5 mM glutamax and pen/strep (without FBS) twice a week for 3 weeks. Cells were maintained at 37 °C in a humidified atmosphere containing 5% $CO_2$.

### 2.5. $^{14}$C-MeAIB transport studies in vitro

Uptake studies were performed using primary neuron-enriched hippocampal cultures at 19–21 days of maturation *in vitro* (DIV). Cells were first rinsed in buffer (2 ml) containing 125 mM NaCl, 4.8 mM KCl, 25 mM HEPES (pH 7.4), 1.2 mM $KH_2PO_4$, 2.5 mM $MgSO_4$, 5.6 mM glucose, and 1 mM EGTA (N buffer). The medium was then replaced with same buffer but without EGTA and containing 2.5 mM $CaCl_2$ (or with N buffer) and pre-incubated for 2 min ( ± inhibitors) at 37 °C. Spontaneous $^{14}$C-MeAIB transport measurements ( ± inhibitors) were then conducted over 15 min of uptake at 37 °C. For the initial drug screening assays, riluzole derivatives (20 μM, screen #1; 10 μM, screen #2) were directly mixed with $^{14}$C-MeAIB and added to the cells. For accurate determination of $IC_{50}$ values for these inhibitors, we preincubated the cells for 2 min in $Ca^{2+}$-containing buffer with various concentrations of the SKA inhibitors and then replaced the medium with the same buffer (+inhibitor) containing $^{14}$C-MeAIB. Low concentrations of MeAIB (3.4–23.4 μM) were used in these experiments to enable a high-affinity transporter system to be more selectively studied. Total levels of $^{14}$C-MeAIB (56.4 mCi/mmol; PerkinElmer) were ~380,000 DPM/well. For substrate competition studies, various concentrations of unlabeled MeAIB (7.8 μM–250 μM) or Gln (31.25 μM–1000 μM) were mixed with $^{14}$C-MeAIB (3.4 μM). For kinetic analysis, we first measured the time-course of uptake to verify that 15 min uptake is within the linear range to record initial velocity and determine accurate $K_m$ and $V_{max}$ values. Following 15 min of spontaneous MeAIB uptake at 37 °C, the cultures were removed from the 37 °C incubator, placed on ice, and washed with ice-cold N buffer (2.5 ml). SDS (1%, 2 ml) was then added to solubilize the cells and the amount of radioactivity was determined by liquid scintillation counting (EcoScint, Nat. Diag.). Untreated cultures and cultures treated with TTX (1 μM), verapamil (25 μM), riluzole (10 μM) and uptake in the absence of $Ca^{2+}$ ions, or at 4 °C, (*i.e.*, background) were used to determine signal:noise to isolate activityregulated, high-affinity MeAIB/Gln transport activity. Background values were subtracted from total $^{14}$C-MeAIB uptake levels to determine levels of neural activity-regulated transport. The n values indicated represent data from independent neuronal cultures.

### 2.6. KA-induced SE and drug treatment

Rats were habituated for at least four days following their arrival and randomly assigned to groups (sham, KA-treated or drug-treated). We used two drug treatment protocols with rats receiving drug before KA administration or rats receiving drug after KA-induced SE. In the first drug treatment protocol, seizures were produced in rats that were injected intraperitoneally (i.p.) with KA (5 mg/kg/h x 2 h in saline; ~500 μL/injection). Drug-treated rats were injected with SKA-378 (30 mg/kg/h x 2 h in Caprylic/Capric triglyceride)

beginning 30 min before KA administration. In the second drug treatment, rats were injected with KA (5 mg/kg/h) until SE was documented. Rats were then injected with 30 mg/kg of SKA-378, SKA-376, SKA-377 or SKA-379 or with 10 mg/kg of riluzole, SKA-41, SKA-378, SKA-377 or SKA-379 at 1 h and 4 h after rats reached SE and once *per* day for 2 d until perfusion on day 3. Seizure severity was assessed using the established five stages of seizure activity in the Racine Scale (Racine, 1972): (0) No behavioral change, (1) Mouth and facial movements (orofacial movements), (2) Head nodding (head myoclonus and/or severe orofacial movements), (3) Forelimb clonus, (4) Rearing and, (5) Rearing and falling with loss of postural control. Once SE is initiated (stage 5), SE events are observed recurrently for up to 4 h.

### 2.7. Fixation and tissue processing

Three days following KA administration the rats were deeply anesthetized using isoflurane and transcardially perfused with 0.9% saline for 5 min followed by 4% paraformaldehyde for 20 min. The brains were removed and post-fixed in paraformaldehyde overnight at 4 °C. The following day the brains were cut coronally anterior and posterior to the hippocampus and post fixed again in 4% paraformaldehyde overnight at 4 °C. The brains were then removed from the paraformaldehyde solution and transferred to 15% sucrose overnight at 4 °C and then followed by 30% sucrose overnight at 4 °C. Brains were then frozen in OTC mounting medium on dry ice and stored at −80 °C until use.

### 2.8. Fluoro-jade B (FJB) labeling

FJB labeling was performed in brain sections of rats saline perfused, paraformaldehyde-fixed, sucrose cryopreserved and frozen. Rat brains were sectioned at Bregma levels (−3.3 to −3.8) to obtain the entire medial hippocampus and other forebrain areas in this region including the cerebral cortex, pyriform cortex, entorhinal cortex, thalamus and amygdala. Brain sections were cut at 25 μm using a cryostat and then transferred to petri dishes filled with room temperature 1 x PBS until sectioning is completed and then mounted onto gelatin coated Fisher Superfrost Plus slides. Excessive liquid was removed, and the slides were airdried for 30 min at 37 °C and then incubated in 4% PAF vapor for 30 min at 37 °C. Slide mounted sections were then immersed in a solution of 1% sodium hydroxide in 80% ethanol for 5 min and then transferred to 70% ethanol for 2 min followed by deionized water for 1 min. Sections were then added to a solution of 0.06% potassium permanganate for 10 min on a rocker, rinsed in deionized water for 1 min then transferred to the FJB Working Solution (0.0004% solution dissolved in 0.1% acetic acid) containing 4’,6-diamidino-2-phenylindole (DAPI; 10 μg/ml) for 20 min. Following staining, slides were rinsed in deionized water (3 × 1 min), dried at 37 °C (~30 min), cleared in xylene (2 × 1 min) and cover-slipped with mounting medium DPX (Sigma-Aldrich).

### 2.9. NeuN immunohistochemistry (IHC)

Rat brains were sectioned at 20 μm using a cryostat and then transferred to petri dishes filled with room temperature 1 x PBS until sectioning is completed. Sections were then transferred to ice cold methanol for 10 min on ice and then to fresh 1 x PBS for rehydration. Sections were then transferred to an ice-cold sodium borohydride (0.1% in 1 x PBS) solution for 5 min followed by three rinses with 1 x PBS. After that, sections were transferred to 12-well

plates and incubated for 1 h in blocking buffer containing 3% bovine serum albumin, 10% donkey serum and 0.25% Triton X in 1 x PBS at room temperature. The medium was then replaced with blocking buffer that contains the monoclonal primary antibody (1:1000) for NeuN (MAB377; Millipore) and incubated overnight at 4 °C. Sections were then washed (5 min intervals) with sequential washes (3 × 1 ml) of PBS-Tween (0.5%), 1 x TBS-Tween (0,5%), and 1 x PBS (3 × 1 ml) at room temperature. Sections were then incubated for 30 min in blocking buffer (diluted 3 x fold in PBS) at room temperature and the sections were then incubated in fresh buffer with a species-specific and highly cross-adsorbed secondary antibody (1:600) coupled to Alexa 594 (Molecular Probes) for 1 h at room temperature. The sections were washed again as described above, and then mounted onto Fisher Superfrost Plus slides and cover slipped using Prolong antifade mounting medium (Invitrogen).

### 2.10. Imaging/quantification

FJB and NeuN stained slides are imaged using a Leica (Nussloch, Germany) DMRXA automated upright inflorescent microscope, a Sensicam QE charge-coupled device digital camera (Cooke Corporation, Romulus, MI), and a filter set suitable for Alexa Fluorophores 488 and 594 (Molecular Probes). Images of sham, KA-treated and the drug-treated groups were obtained at the same exposure time for FJB (300 ms; green), NeuN (300 ms; red) or DAPI (3000 ms; blue). Quantification of neuronal cell damage by FJB staining and neural survival by NeuN fluorescence intensity was performed using Image J: FIJI. The images were uploaded to FIJI and then were split by color channels into separate images (green, blue, and red). The drawing tools selected fixed areas in the CA3, CA1, CA4 hippocampal areas and the DG itself for NeuN and then the fluorescent intensity of that area was quantitated and compared. The background fluorescent intensity was measured by selecting a similar fixed area free of labeled cells. The results were then transferred to Microsoft Excel and the Corrected Total Cell Fluorescence (CTCF) was calculated using the formula CTCF = Integrated Density (IntDen) - (Area of Selected Cell x Mean Fluorescence of background reading) for each hippocampal area. For the FJB + DAPI stained sections, DAPI is only used to visualize and locate hippocampal subregions. Quantification of FJB fluorescent intensity was performed on the pyramidal neuron cell body layers (CA1, CA3 and CA4) as indicated along with the entire hippocampus.

### 2.11. Statistical analysis

Statistical analysis was performed using GraphPad Prism software version 7.0 (GraphPad Software Inc). For initial drug screening of riluzole derivatives *in vitro* the differential potencies of the various compounds were analyzed by ANOVA. The most active compounds identified were used for detailed SAR relationship by analyzing their concentration-response and inhibitory potency ($IC_{50}$ values; ± SEM). All transport experiments were performed in at least 3 independent neuronal culture preparations and analyzed by repeated analysis of variance (ANOVA). Seizure severity was expressed as average Racine seizure score and assessed using ANOVA, with Tukey's multiple comparison test to correct for multiple comparisons. Fluorescent intensity of NeuN and FJB staining in the CA1, CA3 and Hilar/CA4 regions are presented visually as representative sections. Mean fluorescent intensity of NeuN labeling and FJB staining in the CA pyramidal neuron subfields (CA1-4) and in the DG was quantitated. ANOVA was performed on these IHC data and Dunnett's

procedures to correct for multiple comparisons to analyze the results. A value of $p < 0.05$ was regarded as statistically significant.

### 2.12. Pharmacokinetic analysis

All compounds were dissolved in Miglyol 812 neutral oil (caprylic/capric triglyceride; Trade name Neobee M5, Spectrum Chemicals, Gardena, CA, USA) at 1 mg/ml. SKA-41 was gavaged at 10 mg (n = 3) and 30 mg/kg (n = 3). SKA-376, SKA-377 and SKA-378 were injected i.p. at 30 mg/kg (n = 3) or gavaged at 30 mg/kg (n = 3). At 30 min, 1 h, 2h, 4 h, 8h and 24 h after the gavage or i.p. administration, roughly 100–200 μL of blood was collected into EDTA blood sample collection tubes from a tail nick or the tail vein. Plasma was separated by centrifugation. After a washout period of 5 or 7 d the rats were reused, and compound administered again i.p. at 30 mg/kg (n = 6) and three rats sacrificed at 30 min and three rats sacrificed at 60 min to remove plasma and brain to obtain brain:plasma ratios. In another experiment SKA-41, SKA-376, SKA-377 and SKA-378 at 30 mg/kg were administered 1 h after KA-induced SE and plasma and forebrain tissue samples prepared at 4 h after drug administration (n = 3 per compound). For comparison brain and plasma samples were also obtained from rats not treated with KA at 4 h after compound administration. All brain and plasma samples were stored at −80 °C pending analysis. Sample preparation and LC/MS analysis are described in detail in the Supplemental Chemistry section. Plasma protein binding was determined with rat plasma using rapid equilibrium devices (RED, Fisher Scientific) according to the manufacture's protocol.

### 2.13. Sodium channel electrophysiology

NIE neuroblastoma cells that endogenously express the $Na_V1.2$ subtype at high levels and HEK cells transiently transfected with $Na_V1.6$ were voltage clamped by whole-cell patch-clamp using an EPC-10 amplifier and Pulse software (HEKA, Lambrecht/Pfalz, Germany). All experiments were conducted at room temperature (22–24 °C). Cells were bathed in extracellular solution containing (in mM): 160 NaCl, 4.5 KCl, 1 $MgCl_2$, 2 $CaCl_2$ and 10 HEPES; pH was adjusted to 7.4 using NaOH (310 mOsm). Pipettes were pulled from 1.5 mm capillary tubing and filled with intracellular solution containing (in mM) either: 145 KF, 2 $MgCl_2$, 10 EGTA and 10 HEPES (pH adjusted to 7.2 with KOH; 300 mOsm) or 145 CsF, 3 KCl, 2 NaCl, 1 $MgCl_2$, 3 Na-ATP, 0.2 Na-GTP, 10 EGTA and 10 HEPES (pH adjusted to 7.4 with KOH; 303 mOsm). Pipette tip resistances were 2–4 MΩ. Series resistances of 3–10 MΩ were compensated 40–80%. Cells were voltage clamped to a holding potential of −80 mV. $Na^+$ currents were elicited by 50-ms voltage steps from −90 mV to 0 mV applied every 10 s. The sampling frequency was 5 kHz. $IC_{50}$ values for inhibition of $Na_V1.2$ and $Na_V1.6$ sodium channel function by riluzole and our active *in vitro* compounds (SKA-41, SKA-75, SKA-376, SKA-377, and SKA-378) were fitted with Origin 9.0 (OriginLab, Northampton, MA). IGOR-Pro (Wavemetrics, Lake Oswego, OR) was used for current plotting.

## 3. Results

### 3.1. Development of novel aminothiazole riluzole derivatives that inhibit neural activity regulated, high affinity MeAIB transport in mature hippocampal neurons in vitro

A neural activity regulated MeAIB transport activity in mature neuron enriched hippocampal cultures that is potently inhibited by riluzole with ~1 μM affinity has recently been described (Erickson, 2017). Here, we report that the total level of spontaneous MeAIB transport after 15 min in $Ca^{2+}$-containing (2.5 mM) Krebs-based medium into mature rat hippocampal neurons (DIV 19–21) at 23.4 μM external $^{14}$C-MeAIB concentration was 619±21 pmol/well and was inhibited in the presence of the $Na^{+}$-channel blocker TTX (1 μM; 150 ± 15 pmol/well), the $Ca^{2+}$ channel blocker verapamil (25 μM; 119 ± 9 pmol/well), riluzole (10 μM; 133 ± 8 pmol/well) or by the absence of extracellular $Ca^{2+}$ (152 ± 8 pmol/well). Similar inhibition of transport by TTX, verapamil, riluzole, or the absence of external $Ca^{2+}$ ions, was observed using 5.4 μM $^{14}$C-MeAIB concentration (Fig. 1A). Thus, ~80% of the total uptake of MeAIB observed here at either 5.4 or 23.4 μM external $^{14}$C-MeAIB concentration is eliminated by these inhibitors of presynaptic neurotransmission. Transport activity observed at 4 °C was minimal (DPM values ~600) compared to values for total $^{14}$C-MeAIB transport activity (DPM values ~14,000) at 5.4 or 23.4 μM and was subtracted from total uptake levels. $Ca^{2+}$-dependent MeAIB transport is defined here as total uptake minus uptake in the absence of $Ca^{2+}$ ion. $Ca^{2+}$-independent transport has 4 °C DPM values subtracted as background. Transport experiments involving selective $Na^{+}$ channel inhibition includes TTX (1 μM) as background and was subtracted. The % inhibition of activity regulated transport for TTX (1 μM), verapamil (25 μM) or in the absence of $Ca^{2+}$ ($-Ca^{2+}$) were not different from each other and thus, any of these blockers of activity regulated transport can serve as negative controls (*i.e.*, background) to subtract from total uptake levels to isolate, characterize and define this neural activity regulated MeAIB/Gln transport system in mature hippocampal neurons *in vitro*.

Here, we also report the kinetic analysis of spontaneous, activity regulated MeAIB transport in mature hippocampal neuron enriched cultures (DIV 19–21). We have previously reported a $K_m$ value of ~40 μM of MeAIB for a brief (5 min) high KCl (60 mM) stimulated MeAIB transport activity in mature neurons *in vitro* using a Lineweaver-Burke analysis (Erickson, 2017). First, we performed a time-course of spontaneous $Ca^{2+}$-dependent and $Ca^{2+}$-independent MeAIB transport (5.4 μM) activity in mature hippocampal neural networks *in vitro* (DIV~21) to demonstrate that a 15-min uptake period is within the linear range of transport activity, which is required for accurate initial velocity measurements (Fig. 1B). We determine that the $K_m$ for spontaneous $Ca^{2+}$-dependent MeAIB transport is 61 ± 5 μM (n = 3) using Michaelis-Menten analysis (Fig. 1C). We also determined the kinetics of $Ca^{2+}$-independent MeAIB transport under these conditions and find the $K_m$ for MeAIB transport is ~8 times higher (474 ± 31 μM n = 3) likely representing uptake by low affinity MeAIB transporters such as SNAT1 and/or SNAT2 that are expressed in cell bodies and proximal dendrites of neurons in the brain (Mackenzie et al., 2003; Weiss et al., 2003; Melone et al., 2004, 2006). The maximal velocity ($V_{max}$) at 15 min of uptake for $Ca^{2+}$-dependent and $Ca^{2+}$-independent MeAIB transport is 1605 ± 139 and 1793 ± 131 pmol/well, respectively indicating that the maximal capacity of these distinct MeAIB transport systems

are similar in these mature hippocampal neuronal cultures. To determine the affinity of Gln for spontaneous, neural activity regulated high-affinity MeAIB transport we examined the ability of unlabeled Gln to compete with MeAIB for this $Ca^{2+}$-dependent activity (Fig. 1C). Spontaneous $^{14}$C-MeAIB (5.4 μM) transport is inhibited by unlabeled MeAIB with relatively high affinity ($IC_{50}$ 50 ± 6 μM; n = 6) in this assay, as expected. Gln also competes with $^{14}$C-MeAIB but at lower potency ($IC_{50}$ 162 ± 17 μM; n = 9), which is still within the range of reported values of Gln in brain extracellular space (Kanamori and Ross, 2004, 2011, 2013). These results further establish that a spontaneous, neural activity regulated, high affinity MeAIB/Gln transporter exists in mature hippocampal neuronal networks *in vitro* and that its transport activity is expressed on the plasma membrane in a neural activity regulated and $Ca^{2+}$-dependent manner (Fig. 1D).

In this study, we used our assay of spontaneous, activity regulated high affinity MeAIB/Gln transport in mature hippocampal neurons as a screen to identify novel riluzole derivatives that inhibit this activity with similar affinity as riluzole. We first confirmed that riluzole inhibits spontaneous, neural activity regulated, high affinity MeAIB transport with micromolar affinity ($IC_{50}$ = 860 ± 20 nM), as previously reported (Erickson, 2017). We started by screening a library of riluzole derivatives (Library 1, Fig. 2A), which was originally developed to find activators of $Ca^{2+}$-activated $K^+$ channels (Sankaranarayanan et al., 2009). Compounds were added together with $^{14}$C-MeAIB (23.4 μM) in this assay and spontaneous transport activity was measured after 15 min in $Ca^{2+}$-containing (2.5 mM) Krebs-based medium. This screen of Library 1 revealed 8 inhibitors that blocked high affinity MeAIB transport activity by more than 90% when tested at a concentration of 20 μM (Fig. 2B). Most of these compounds (SKA-3, SKA-7, SKA-11, SKA-19, SKA-32, SKA-45 and SKA-51) were discarded because of their close structural similarity to riluzole. SKA-41 was the only unique structure among these compounds being the only aminothiazole tested here as compared to the rest, which are all benzothiazoles. A search for reported biological activity for SKA-41 in the SciFinder Chemical Abstract System only revealed the previously published finding that SKA-41 is inactive on $Ca^{2+}$-activated $K^+$ channels (Sankaranarayanan et al., 2009). A preliminary study of SKA-41 pharmacokinetic properties revealed that the compound exhibits excellent brain penetration and oral availability (*see* below).

We then tested a second compound library (Library 2, Fig. 3A) containing 27 derivatives of SKA-41 that were either purchased or synthesized previously (Shim et al., 2019) for their ability to block spontaneous, neural activity regulated MeAIB transport at 10 μM. Eight compounds, which all contained a larger, more lipophilic naphthalene substituent instead of the phenyl substituent of SKA-41, were identified as active (Fig. 3B). Indeed, all of these active compounds identified here are chemically derived from the two regioisomers SKA-75 or SKA-76 that exhibited intermediate potency of ~50% block at 10 μM and both have unsubstituted naphthalene rings (Fig. 3A). SKA-219, a brominated derivative of SKA-75, was initially a favorite because it inhibited activity regulated MeAIB transport in mature hippocampal neurons by >95% at 10 μM. The other active compounds we identified in this second screen were the SKA-75 derivatives SKA-190, SKA-193, and SKA-247 and the SKA-76 derivatives SKA-198 and SKA-220 (Fig. 3, Table 1).

While SKA-219, the brominated SKA-75 derivative, was attractive because of its potency for inhibiting spontaneous, neural activity regulated MeAIB transport (Fig. 4A) we had concerns about its structure. Heavy halogens like bromine and iodine in drugs have been associated with phototoxicity, photoreactivity, reactive metabolite formation, *etc.* that can lead to safety issues (Stepan et al., 2011). Brominated compounds are also typically poorly soluble because of their high logP values, which makes formulation and drug administration challenging. We therefore synthesized the chlorine substituted SKA-376, SKA-377, SKA-378 and SKA-379 compounds that were obtained by reacting active compounds SKA-41, SKA-190, SKA-75 and SKA-76, respectively, with 2-chloro-1,3-bis(methoxycarbonyl)guanidine (Palau'Chlor®), which is a highly reactive chlorinating agent that is ideal for introducing chlorine substituents in predictable locations on heterocycles (Rodriguez et al., 2014) (Supplemental data Scheme A). We found that SKA-378 inhibited spontaneous neural activity regulated MeAIB transport *in vitro* as potently as riluzole, SKA-219, and SKA-375, the brominated derivative of SKA-190 (Fig. 4).

We report the concentration response relationship of all 12 of these active naphthalenyl substituted aminothiazoles derived from SKA-75 or SKA-76 that we have identified to block spontaneous activity-regulated $^{14}$C-MeAIB transport activity in mature hippocampal neurons *in vitro,* compared to riluzole (Table 1). We find that SKA-378 was as potent as riluzole to inhibit spontaneous high affinity MeAIB transport activity ($IC_{50}$ 1.1 ± 0.17 μM). SKA-377, the chlorinated derivative of SKA-190 exhibited potency similarly to SKA-378, ($IC_{50}$ 1.7 ± 0.26 μM). SKA-376, the chlorinated derivate of SKA-41 and SKA-379, the chlorinated derivative of SKA-76 were less potent ($IC_{50}$ ~4–6 μM) to inhibit spontaneous high affinity $^{14}$C-MeAIB transport activity similar to SKA-75 and SKA-76 ($IC_{50}$ ~5–6 μM) (Fig. 4, Table 1).

### 3.2. SKA-378 prevents neural injury in the hippocampus when given before KA-induced SE

The KA model of TLE in rats can be generated by i.p. injection of KA, the presynaptic glutamategic excitotoxin that produces stage 5 grade seizure activity (*i.e.,* SE) based on the Racine scale (Racine, 1972). We confirm that KA-induced SE results in acute hippocampal neural injury by 3 d (Fig. 5). We used FJB staining in brain sections *in situ* to evaluate levels of KA-induced degeneration in the hippocampal pyramidal neuron layer subfields (Schmued and Hopkins, 2000). In sham rats, FJB labeling is not observed in the hippocampus. In KA treated rats, FJB fluorescence intensity is specifically increased in neurons of the CA3, CA1 and CA4 (within the DG hilus) subfields in the hippocampus after 3 d (Fig. 5A,B,C) indicating neural injury. High-power images of FJB labeling in these hippocampal subfields reveal specific cell body labeling (Fig. 5D). FJB fluorescence in degenerating neurons confirm that KA-induced injury includes neurons in the vulnerable CA subfields of the hippocampus in our hands.

SKA-378 was one of the most potent compounds that inhibit spontaneous, neural activity regulated MeAIB/Gln transport, as effectively as riluzole, and preliminary pharmacokinetic analysis revealed that SKA-378, like SKA-41, exhibited excellent bioavailability and brain

penetrance (*see* below). Thus, SKA-378 was chosen to be examined first for neuroprotection studies *in vivo.* We examined if SKA-378 could prevent hippocampal neural injury produced by KA (5 mg/kg/h x 2 h). Here, SKA-378 (30 mg/kg) was given twice; 30 min before the first dose of KA (5 mg/kg) and 30 min after the second dose of KA (5 mg/kg). We find that such pretreatment with SKA-378 was only moderately effective to reduce seizure activity as >50% of the rats treated with SKA-378 still exhibited maximal stage 5 seizures on the Racine scale (*i.e.*, SE), while the other SKA-378 pretreated rats reached at least stage 2–3 seizures that included wet dog shakes, staring, *etc.* Pretreatment of rats with SKA-378 did not show a significant reduction in seizure severity compared to non-treated KA-injected rats (Tukeys analysis; $p = 0.5686$) (Fig. 6D). Nevertheless, we examined neural injury in the hippocampus 3 d after KA administration in sham, KA treated, and SKA-378 pretreated rats. We report the results from sections containing the medial hippocampal region (Bregma −3.3 to −3.8). We find that SKA-378 pretreatment blocks neuronal hippocampal injury induced by KA as indicated by the absence of FJB staining in all of the CA pyramidal neuron cell layers (CA3: $F(2,18) = 28.62$; $p < 0.0001$; CA1: $F(2,18) = 9.417$; $p = 0.0016$; CA4: $F(2,18) = 17.19$; $p < 0.0001$) (Fig. 6A). The neuroprotection afforded by SKA-378 pretreatment in the hippocampus was also assessed by NeuN immunofluorescence. NeuN is a selective marker of neuronal cell bodies in the brain that delineate the hippocampal subfields including the CA and DG neuronal cell body architecture *in situ* and so its expression level reflects neuronal viability (Mullen et al., 1992). In sham rats, NeuN staining reveals intact neuronal architecture in all hippocampal subfields (Fig. 6C). NeuN expression in CA3, CA1, and CA4 subfields is markedly lower in KA-treated rats as measured by greatly decreased fluorescence intensity by IHC (Fig. 6C). DG neurons are not vulnerable to KA toxicity which is consistent with the absence of FJB labelling in these neurons (Fig. 6A) and NeuN fluorescent labeling is intact and not different from sham or SKA-378 pretreated rats (Dunnett's analysis: $F(2, 18) = 0.1387$; $p = 0.8715$) following KA treatment (Fig. 6C). FJB fluorescence in degenerating neurons and NeuN labeling of surviving neurons confirm that KA-induced injury includes neurons in the vulnerable CA subfields of the hippocampus. NeuN labeling in SKA-378 treated rats showed clear pyramidal neuron delineation of CA4 ($F(2,18) = 15.55$; $p < 0.0001$) (DG hilar region), CA3 ($F(2,18) = 27.18$; $p < 0.0001$) and CA1 ($F(2,18) = 20.59$; $p < 0.0001$) subfields with fluorescent intensity in these areas nearly identical to sham levels (Fig. 6C). Quantification of the fluorescent intensity of FJB and NeuN labeling in the entire hippocampus and in the CA3, CA1 and CA4/hilar region are shown in Fig. 6B (FJB) and Fig. 6D (NeuN) and reveal that SKA-378 is a neuroprotective agent against acute KA-induced neural injury.

### 3.3. Riluzole and the novel chlorinated aminothiazoles SKA-377, SKA-378, and SKA-379 attenuate neural injury in the hippocampus when given after KA-induced SE

While SKA-378 could not prevent KA-induced SE in all animals, all SKA-378 pretreated animals were still protected from KA-induced hippocampal neural injury at 3 d. We therefore examined if SKA-378 could prevent neural injury if administered after KA-induced SE occurs (Fig. 7), which is more clinically relevant. Rats were treated with KA (5 mg/kg/h) and 1 h after SE was documented (Racine 5 stage) they were treated with SKA-378 (30 mg/kg), then again with SKA-378 4 h after SE, and then once a day for the next two days by i.p. administration. The duration of KA-induced SE events was between

4 and 6 h after the onset SE and was not affected by SKA-378. We examined neural injury by FJB staining and NeuN immunoreactivity by fluorescence microscopy 3 d post-KA treatment in the medial hippocampal sections as described above. Representative images of FJB staining in sham, untreated (KA) and post-SE drug treated (30 mgkg) rats (SKA-378, SKA-377, SKA-379 and SKA-376) are shown in Fig. 7A. In post-SE SKA-378 treated rats, FJB staining in hippocampal CA1-4 neurons was minimal (CA3: $F(5,42) = 16.51$; $p < 0.0001$; CA1: $F(5,42) = 3.807$; $p = 0.0062$; CA4: $F(5,42) = 8.167$; $p < 0.0001$) and similar to that observed in SKA-378 pre-treated rats (Fig. 7B). SKA-378 treatment after SE in this way also largely prevents the diminished NeuN fluorescence normally caused by KA in all pyramidal neuron subfields of the hippocampus (CA3: $F(5,42) = 12.27$; $p < 0.0001$; CA1: $F(5,42) = 5.565$; $p = 0.0005$; CA4: $F(5,42) = 6.586$; $p = 0.0001$) similarly to SKA-378 pretreated rats (Fig. 7C) further demonstrating the acute neuroprotection provided by SKA-378. SKA-376 did not significantly reduce neural injury in the hippocampal subfields as measured by both FJB staining and by NeuN fluorescence (Fig. 7B and C). On the other hand, SKA-377 and SKA-379 were neuroprotective against KA induced hippocampal neural injury when given post-SE, similar to SKA-378 ($F(5,42) = 11.28$; $p < 0.0001$) (Fig. 7B and C). We next examined the neuroprotection afforded by these novel compounds at 10 mg/kg, which is the average dose of riluzole that is generally used for neuroprotection studies (Fig. 8). Higher doses of riluzole (*e.g.,* 30 mg/kg) render rats immobile and unresponsive, unlike SKA-378. Representative images of FJB staining in untreated (KA) and post-SE drug treated (10 mgkg) rats (SKA-378, SKA-377, SKA-379, SKA-41, and riluzole) are shown in Fig. 8A. We report that SKA-379, SKA-378, SKA-377 and SKA-41 administered at 10 mg/kg are neuro-protective, but not as protective as riluzole ($F6,44) = 8.159a$; $p < 0.0001$) (Fig. 8B) which prevents acute neural injury altogether. Riluzole also shortened the duration of KA-induced SE events to less than 2 h and the rats then appeared to be relatively immobile/sedated. A reduced level of neuroprotection observed at 10 mg/kg compared to 30 mg/kg of our most active aminothiazole compounds demonstrate a dose dependence, which is important to identify optimal dosage for acute administration.

### 3.4. SKA-378 reduces neural injury in associated hippocampal limbic areas caused by KA-induced SE

We used FJB staining *in situ* to evaluate levels of KA-induced degeneration in hippocampal interconnected limbic regions. We observed extensive FJB labeling following KA-induced SE in neurons of the piriform and entorhinal cortex and in neurons of the midline thalamus and basolateral amygdala areas (Supplemental data), as reported previously (Hopkins et al., 2000; Srivastava et al., 2020). Pretreatment of rats with SKA-378 as described above greatly reduced FJB staining in these hippocampal limbic areas (Supplemental data). Riluzole (post-treated) largely prevented neural injury in these limbic areas (*not shown*).

### 3.5. Pharmacokinetics and plasma:brain ratios

The plasma time courses and plasma:brain ratios for SKA-41, SKA-378, SKA-377, and SKA-376 are shown in Fig. 9. The plasma concentration profiles of all tested compounds reveal excellent bioavailability for these compounds, with oral and i.p. application of 30 mg/kg achieving nearly identical exposure levels (= areas under the plasma curve) and plasma peak concentrations of 8–12 μM. All of these compounds were also highly brain

penetrant as demonstrated by the total brain concentrations (>10 μM) that equaled or exceeded total plasma concentrations at 30 min, 1 h and 4 h after i.p. application. In keeping with their lipophilicity, SKA-376, SKA-377 and SKA-378 are all highly plasma protein bound with free concentrations ranging between 0.5 and 1% (*see* Table 1). In contrast to riluzole, which has a brain:plasma ratio of 1 (Coleman et al., 2015; Colovic et al., 2004) the original compound identified here, SKA-41, reached 7-fold higher concentrations in the brain than in the plasma (Fig. 9B). SKA-377 and SKA-378 were also found to have excellent oral availability when administered by gavage at 10 and 30 mg/kg (Fig. 9C,E).

To assess whether KA-induced seizure activity affects the brain penetration of these compounds we examined the brain:plasma ratios in rats 4 h after they exhibited KA-induced SE (Fig. 9). Rats were treated with SKA-41, SKA-376, SKA-377 and SKA-378 (30 mg/kg) once 1 h after SE and then harvested for plasma and brain after 4 h. This paradigm is similar to what we used for the *in vivo* neuroprotection studies post-SE KA treatment described above; although at 4 h post-SE in neural protection studies above we injected a second dose of compounds. Total brain levels of all four compounds at 4 h post SE (see grey shading in Fig. 9B,D,E,H) were somewhat higher than at 4 h after a single administration, but the presence of KA, which presumably opens up the blood brain barrier (Zucker et al., 1983; Pont et al., 1995), did not change the brain:plasma ratios of any of these lipophilic compounds.

### 3.6. On the mechanism of inhibition of spontaneous, activity-regulated high-affinity MeAIB transport by SKA-378 and riluzole

In this study, we also seek to identify potential mechanisms involved in the inhibition of $Ca^{2+}$-regulated MeAIB/Gln transport activity in hippocampal neurons *in vitro* by riluzole and our novel aminothiazole derivatives of riluzole that may relate to their acute neuroprotective properties *in vivo.* For this, we first examined whether riluzole and SKA-378 are competitive or non-competitive inhibitors of spontaneous, neural activity regulated high affinity MeAIB transport activity in mature hippocampal neuronal circuits *in vitro.* We performed Michaelis-Menten kinetic analysis of SKA-378 and riluzole's inhibitory action on $Ca^{2+}$-regulated MeAIB transport activity *in vitro* and find that inhibition is noncompetitive because both riluzole and SKA-378 cannot compete at the substrate recognition site on the transporter (Fig. 10A). Eadie-Hofstee analysis indicates the $K_m$ values for MeAIB in control (61 ± 5 μM), +SKA-378 treated (58 ± 6 μM) and +riluzole treated (63 ± 6 μM) are not different (n = 3). While SKA-378, and riluzole, at 1 μM concentration do not affect the $K_m$ of spontaneous, activity-regulated $^{14}$C-MeAIB transport activity these compounds reduce the maximal velocity ($V_{max}$) of transport. The $V_{max}$ values for SKA-378 (73 ± 6 pmol/min) and riluzole (54 ± 1 pmol/min) are roughly 50% less than observed for control $Ca^{2+}$-regulated MeAIB transport values (107 ± 9 pmol/min) (Fig. 10B). These kinetic results indicate that riluzole and our novel aminothiazoles (*e.g.,* SKA-378) act *via* indirect mechanisms to inhibit spontaneous, neural activity regulated high affinity MeAIB/Gln transport activity in mature hippocampal neuron-enriched cultures. Our results support the concept that neural activity regulated, $Ca^{2+}$-dependent cycling of the transporter involved here, from intrasynaptic stores to the plasma membrane, exists in

mature hippocampal neuronal cultures that could be targeted for neuroprotection (*see* Fig. 1D).

A principal target of riluzole for neuroprotection is believed to be the inhibition of $Na^+$ channel activity in neurons and we have previously reported that TTX (1 μM) eliminates spontaneous neural activity regulated MeAIB transport activity (Erickson, 2017), and that is also confirmed here (Fig. 1A). Therefore, we examined the inhibitory potencies of TTX itself and a derivative of TTX reported to be more selective for the $Na_V1.6$ isoform (Teramoto and Yotsu-Yamashita, 2015), which is enriched in mature forebrain excitatory neurons compared to the $Na_V1.2$ isoform that is expressed earlier but is replaced by $Na_V1.6$ during neuronal maturation (O'Malley and Isom, 2016; Meisler et al., 2021). We find that TTX exhibits an $IC_{50}$ inhibitory potency of 1.7 ± 0.2 nM (n = 5) to block spontaneous activity-regulated MeAIB transport activity in hippocampal neuron cultures. The $Na_V1.6$ inhibitor 4,9-anhydroTTX exhibits an $IC_{50}$ inhibitory potency of 61 ± 4 nM (n = 3) to block activity in neurons *in vitro* (Fig. 10C). The inhibitory potency of 4, 9-anhydroTTX on $Na_V1.2$ channels is $IC_{50}$ > 1 μM (Teramoto and Yotsu-Yamashita, 2015; Rosker et al., 2007). Our results indicate that $Na_V1.6$ $Na^+$ channel activity may be critical to drive spontaneous neural activity regulated MeAIB/Gln transport activity in mature hippocampal neurons *in vitro*.

We further examined the inhibitory potencies of riluzole, and the original active aminothiazole identified SKA-41 in our first screen, SKA-75 and SKA-219 in our second screen, and three of our new chemical entities (SKA-376, 377, 378) to inhibit the activity of two major hippocampal $Na^+$ channels $Na_V1.2$ and $Na_V1.6$ in heterologous cell line assays (Fig. 11) using whole-cell patch-clamp. In keeping with some literature reports (Herbert et al., 1994; Song et al., 1997; Stefani et al., 1997; Spadoni et al., 2002), we find that riluzole is a relatively weak $Na_V1.2$ blocker with an $IC_{50}$ of 67 ± 9 μM (Fig. 11A,D). The block is not frequency dependent (Fig. 11C). SKA-378 is even less potent on $Na_V1.2$ with an $IC_{50}$ of 118 ± 13 μM (Fig. 11B,D). This potency sequence was reversed on $Na_V1.6$, which was more potently blocked by SKA-378 ($IC_{50}$ 28 ± 4 μM) than by riluzole ($IC_{50}$ 115 ± 2 μM). The 4,9-anhydroTTX was less potent in our hands ($IC_{50}$ 138 ± 24 nM, Fig. 11E) than previously reported for $Na_V1.6$ expressed in oocytes (Rosker et al., 2007). TTX itself was significantly more potent ($IC_{50}$ 0.426 ± 0.003 nM, Fig. 11E) with values similar to the inhibition of spontaneous, neural activity regulated MeAIB transport (Fig. 10C). SKA-378 is the most potent agent to inhibit $Na_V1.6$ activity and least potent agent to inhibit $Na_V1.2$ activity compared to riluzole and the other active compounds in these heterologous cell assays *in vitro.* (Fig. 11D).

## 4. Discussion

Glutamate (Glu) is the major excitatory transmitter in synaptic vesicles that is released in the brain by $Ca^{2+}$-regulated exocytosis (Maycox et al., 1990; Sudhof, 2012). Glu excitotoxicity and neural injury resulting from KA-induced SE in rodents is an accepted animal model of human TLE. Glu transmission in hippocampal neurons and Glu-induced excitotoxicity requires resupply of the synaptic Glu precursors for continued synthesis and release. Gln has long been thought to be an important precursor to synaptic Glu transmitter synthesis

*via* the Glu/Gln cycle between neuronal synapses and astrocytes especially under intense depolarization conditions in the hippocampus; although the mechanisms involved still remain unclear. Excessive synaptic Glu transmission in the brain results in excitotoxicity, both acutely and chronically, that has long-term consequences for neural degeneration, in general, both *in vitro* and *in vivo*. Neuronal maturation of regulated presynaptic release of Glu and GABA and the excitatory/inhibitory balance required for stable hippocampal networks occurs after 3 weeks *in vitro* and after 3 postnatal weeks in hippocampal circuits *in vivo.* This is because the major synaptic vesicular transporters that control presynaptic excitatory and inhibitory synaptic neurotransmission in these neurons (*i.e.*, VGLUT1 and VGAT) are also up-regulated during this period (Boulland et al., 2004; De Gois et al., 2005; Wilson et al., 2005) and they are required for $Ca^{2+}$-regulated Glu and GABA synaptic transmission (Takamori et al., 2000; Moechars et al., 2006; Saito et al., 2010). The maturation of synaptic Glu neurotransmitter cycling after synaptic release to support continued excitatory transmission also develops during this period (Bolshakov and Siegelbaum, 1995; Wasling et al., 2004; Chowdhury et al., 2007; Hertz, 2013). SE induced neural excitotoxicity in the hippocampus and interconnected limbic regions by KA treatment also requires a mature hippocampal neural network that is similarly established and exists only after the third postnatal week (Nitecka et al., 1984; Wozniak et al., 1991; Haas et al., 2001). Activity regulated MeAIB/Gln transport activity develops during the second and third weeks in hippocampal neural cultures and is maximal after the third week (Erickson, 2017), as well. An important influence in neuro-protection here may arise from the selective expression of the specific transporter protein that mediates neural activity regulated high affinity MeAIB/Gln transport in mature hippocampal excitatory neurons. The vulnerability of the hippocampus to hyperactivation by KA treatment and the prevention of acute neural injury by riluzole and significant attenuation by SKA-378 and SKA-379 in this study suggests that these compounds target a common mechanism that could prevent the propagation of neural injury that leads to epileptic disease within hippocampal limbic circuits.

Riluzole is a benzothiazole anticonvulsant agent that suppresses presynaptic Glu transmission in the brain, by unclear mechanisms because it has multiple targets that could inhibit synaptic excitotoxicity under seizure activity to provide neuroprotection. The most potent action of riluzole and several of our novel naphthalenyl substituted aminothiazoles reported here is inhibition of spontaneous, high affinity MeAIB/Gln transport activity in mature hippocampal neuron enriched cultures *in vitro.* The blockade of $Na^+$ channels in hippocampal neurons is one of the proposed mechanisms of action of riluzole, and $Na^+$ channel blockade is considered a general target of many ASDs such as phenytoin and carbamazepine, and others that are used clinically (Errington et al., 2005; Pal et al., 2021). However, limbic seizures and neurotoxicity induced by KA *in vivo* are resistant to conventional ASDs such a phenytoin and valproic acid (Clifford et al., 1982; Fuller and Olney, 1981). In the KA model of temporal lobe epilepsy (TLE), a potential AED would be administered at least 1 h after the first SE event to prevent acute hippocampal neural injury. Here, we show for the first time that riluzole treatment after KA-induced SE blocks neural injury in the hippocampus. Post KA-induced SE treatment with SKA-378 and SKA-379 attenuate hippocampal neural injury in a similar way, but are less potent. Our data indicate

that riluzole and the aminothiazole derivatives of riluzole described here may offer a new presynaptic approach to prevent neural injury in hippocampal circuits that occurs after KA-induced SE.

Naphthalenyl-substituted aminothiazole derivatives of riluzole are underdeveloped agents for neuroprotection. While the benzothiazole riluzole is relatively safe at low concentrations (Bellingham, 2011) it is not especially brain penetrant (Verma et al., 2016; Pelletier et al., 2018) and has side-effects such as sedation and impaired motor control *in vivo* in rats (Doble, 1996); many ASDs currently used clinically have similar associated side-effects (Perucca and Meador, 2005; Brodie, 2017; Loscher and Klein, 2021). Identifying the targets that protect vulnerable hippocampal neurons require pharmacological agents that can affect sites that are important for prevention of excitotoxic neural injury. Prolonged seizure events induced by KA treatment *in vivo* lead to excessive Glu release and NMDA Glu receptor activation but while postsynaptic Glu receptor therapy prevents neural injury in animal models of many excitotoxic disease states, including epilepsy (Loscher and Schmidt, 2012; Rogawski, 2013; Schidlitzki et al., 2017; Hanada, 2020), NMDA receptor antagonists are not well tolerated in humans because of unacceptable CNS side-effects (Muir, 2006; Lipton, 2004). In addition, while NMDA receptor blockade immediately after a 90 min KA-induced SE is an effective means to reduce the damage produced in several brain regions, including the hippocampus, this partial neuro-protection of the limbic system does not prevent the development of epilepsy (Ebert et al., 2002; Brandt et al., 2003). Thus, it is critical to further develop novel presynaptic neuroprotective agents that can reduce Glu-induced excitotoxic injury in these vulnerable hippocampal and limbic neurons. We report here that the administration of aminothiazoles SKA-377, SKA-378 and SKA-379 (30 mg/kg; i.p.) after KA-induced SE occurs significantly reduce acute neural injury in the hippocampus after 3d. Riluzole blocks neural injury at 10 mg/kg. Thus, riluzole and our novel aminothiazole derivatives of riluzole may be useful agents to further understand the mechanisms involved that can prevent acute Glu-induced neural injury in the hippocampus following SE events and, which otherwise, may lead to the initiation of chronic injury and progression of temporal lobe epilepsy.

The mechanism of acute neuroprotection of hippocampal neurons by riluzole and our novel napthalenyl substituted aminothiazoles following KA-induced SE is not known. Here, kinetic analysis reveals that riluzole and SKA-378 inhibit spontaneous, activity regulated, high affinity MeAIB transport *in vitro* ($IC_{50}$ ~1 μM) by indirect means because they cannot compete at the substrate recognition site for transport activity in neurons. That is, these compounds do not affect the $K_m$ (affinity) but the $V_{max}$ (transporter #) of transport activity at the plasma membrane; although an allosteric mechanism could be involved. TTX and the $Na_V1.6$ antagonist 4,9-anhydroTTX are potent ($IC_{50}$ ~ 1 and 60 nM, respectively) inhibitors of neural activity regulated MeAIB/Gln transport activity in hippocampal neuronal cultures. SKA-378 is the most potent agent to inhibit $Na_V1.6$ activity ($IC_{50}$ ~28 μM) and least potent agent to inhibit $Na_V1.2$ activity ($IC_{50}$ ~118 μM) in heterologous cell assays *in vitro.* Riluzole also inhibits $Na_V1.6$ and $Na_V1.2$ with similar μM affinities but in reverse order of potency in these cell assays. However, the high plasma protein binding of riluzole, SKA-378 and SKA-377 in serum (96–99%) could limit their free brain concentrations to the <1 μM range; although total brain concentrations of several of these active aminothiazoles

compounds are in the >10 μM concentration. Thus, it is unlikely that $Na_V1.6$ inhibition is the major contributor to the neuro-protective effect by riluzole or our aminothiazole riluzole derivatives *in vivo.* However, the evaluation of % free concentrations of our active aminothiazoles, and riluzole, in brain CSF and extrasynaptic space, and compound distribution into phospholipid membrane compartments in synapses, may be necessary in future studies to better evaluate concentration response relationships of these lipophilic drugs *in vitro* and *in vivo* to their neuroprotective targets (Rizk et al., 2017; Treyer et al., 2018). Spontaneous, activity regulated MeAIB transport activity described here is also dependent on $Ca^{2+}$ ion that is required for exocytosis of vesicles that contain Glu. The potency of riluzole and our novel active aminothiazoles in hippocampal neurons may result from their interference with the cycling of the neural activity regulated MeAIB/Gln transporter within Glu terminals to the plasma membrane. A similar scheme of activity regulated, $Ca^{2+}$-dependent cycling of reuptake transporters between synaptic vesicles and the plasma membrane in nerve terminals has been described in other neurotransmitter systems in the brain (Ferguson et al., 2003; Deken et al., 2003).

The relationship between an initial limbic epileptogenic seizure event (*i.e.*, SE) and the resulting neural injury in the hippocampus as a critical step in the progression to temporal lobe epilepsy is not understood. Presynaptic therapies that prevent acute limbic neural injury following an initial SE event (Pitkanen and Sutula, 2002; Guerriero et al., 2015; Saletti et al., 2019) are lacking. We report that riluzole prevents acute KA-induced hippocampal injury when administered after SE is observed for the first time. Novel naphthalenyl substituted aminothiazole derivatives of riluzole also provide acute neuroprotection in this way. However, SKA-378 does not prevent KA-induced SE, nor do the most active aminothiazole compounds (SKA-378 and SKA-379) described here limit the duration of SE following KA treatment, unlike riluzole. We would like to suggest that riluzole, SKA-378 and SKA-379 could serve as tool compounds that could clarify the role of SE-induced acute neural injury in epileptogenesis and epileptic disease using the KA-model of TLE. SE also induces acute and chronic inflammatory processes involving astrocytes and microglia in early and later stages (Vezzani et al., 2011, 2019; Mukhtar, 2020) and it will be important to establish whether riluzole and our novel aminothiazoles can also prevent acute and chronic inflammation following KA-induced SE in future studies. In conclusion, we have found that riluzole and several novel naphthalenyl substituted aminothiazole derivatives of riluzole developed here attenuate acute hippocampal injury following KA-induced SE. Riluzole and these novel aminothiazole compounds have significant scientific value to understand the mechanisms that underlie their prevention of acute hippocampal neural injury following KA-induced SE. In addition, riluzole and these novel aminothiazole derivatives of riluzole could have significant therapeutic value as a preventative measure to be used after an initial SE event occurs to reduce acute hippocampal neural injury that, otherwise, can lead to the progression of epileptic disease.

## Supplementary Material

Refer to Web version on PubMed Central for supplementary material.

## Acknowledgments

This research was supported by the National Institute of Neurological Disorders and Stroke grants NS 109668, NS112788 and NS113955 to JDE.

## Data availability

Data will be made available on request.

## Abbreviation

| | |
|---|---|
| **ALS** | Amyotrophic lateral sclerosis |
| **ANOVA** | Analysis of variance |
| **ASDs** | Antiseizure drugs |
| **AEDs** | Antiepileptic drugs |
| **CTCF** | Corrected total cell fluorescence |
| **CSF** | Cerebral spinal fluid |
| **DAPI** | 4′,6-diamidino-2-phenylindole |
| **DIV** | Days *in vitro* |
| **DG** | Dentate gyrus |
| **DMEM** | Dulbecco's modified eagle medium |
| **EAAT2** | Excitatory amino acid transporter 2 |
| **FJB** | Fluoro-jade B |
| **Glu** | Glutamate |
| **Glt1** | Glutamate transporter 1 |
| **Gln** | Glutamine |
| **KA** | Kainic acid |
| **LC/MS** | Liquid chromatography – mass spectrometry |
| **$V_{max}$** | Maximal velocity |
| **MeAIB** | Methylaminoisobutryic acid |
| **$K_m$** | Michaelis-Menton constant |
| **NB** | Neurobasal medium |
| **NMDA** | *N*-methyl-D-aspartate |
| **Ril** | Riluzole |

| | |
|---|---|
| **SNATs** | Sodium-coupled Neutral Amino Acid Transporters/System N and A Transporters |
| **$Na_V1.2$** | Sodium channel isoform 1.2 |
| **$Na_V1.6$** | Sodium channel isoform 1.6 |
| **SLC38** | Solute carrier family 38 |
| **SE** | Status epilepticus |
| **TLE** | Temporal lobe epilepsy |
| **VGAT** | Vesicular GABA transporter |
| **VGLUT1** | Vesicular glutamate transporter-1 |

## References


Ali R, Siddiqui N, 2013. Biological aspects of emerging benzothiazoles: a short review. J. Chem 12. Article ID 345198.

Bacci A, et al. 2002. Block of glutamate-glutamine cycle between astrocytes and neurons inhibits epileptiform activity in hippocampus. J. Neurophysiol 88 (5), 2302–2310. [PubMed: 12424271]

Bellingham MC, 2011. A review of the neural mechanisms of action and clinical efficiency of riluzole in treating Amyotrophic Lateral Sclerosis: what we have learned in the last decade? CNS Neurosci. Ther 17, 4–31. [PubMed: 20236142]

Ben Ari Y, 1985. Limbic seizure and brain damage produced by kainic acid: mechanisms and relevance to human temporal lobe epilepsy. Neuroscience 14, 375–403. [PubMed: 2859548]

Benassi SK, et al. 2021. Two decades of research toward a potential first anti-epileptic drug. Seizure 90, 99–109. [PubMed: 33714677]

Bittigau P, Ikonomidou C, 1997. Glutamate in neurologic diseases. J. Child Neurol 12, 471–485. [PubMed: 9430311]

Blumcke I, et al. 2012. Defining clinico-neuropathological subtypes of mesial temporal lobe epilepsy with hippocampal sclerosis. Brain Pathol. 22, 402–411. [PubMed: 22497612]

Bolshakov VY, Siegelbaum SA, 1995. Regulation of hippocampal transmitter release during development and long-term potentiation. Science 269 (5231), 1730–1734. [PubMed: 7569903]

Borowicz KK, et al. 2004. Riluzole enhances the anti-seizure action of conventional antiepileptic drugs against pentetrazole-induced convulsions in mice. Pol. J. Pharmacol 56, 187–193. [PubMed: 15156069]

Bouilleret V, et al. 1999. Recurrent seizures and hippocampal sclerosis following intrahippocampal kainate injection in adult mice: electroencephalography, histopathology and synaptic reorganization similar to mesial temporal lobe epilepsy. Neuroscience 89, 717–729. [PubMed: 10199607]

Boulland JL, et al. 2004. Expression of the vesicular glutamate transporters during development indicates the widespread corelease of multiple neurotransmitters. J. Comp. Neurol 480 (3), 264–280. [PubMed: 15515175]

Brandt C, et al. 2003. N-methyl-D-aspartate receptor blockade after status epilepticus protects against limbic brain damage but not against epilepsy in the kainate model of temporal lobe epilepsy. Neuroscience 118, 727–740. [PubMed: 12710980]

Brewer GJ, et al. 1993. Optimized survival of hippocampal neurons in B27-supplemented Neurobasal, a new serum-free medium combination. J. Neurosci. Res 35 (5), 567–576. [PubMed: 8377226]

Brodie MJ, 2017. Tolerability and safety of commonly used antiepileptic drugs in adolescents and adults: a clinician's overview. CNS Drugs 31, 135–147. [PubMed: 28101765]

Chaudhry FA, et al. 2002a. Glutamine uptake by neurons: interaction of protons with system A transporters. J. Neurosci 22 (1), 62–72. [PubMed: 11756489]

Chaudhry FA, Reimer RJ, Edwards RH, 2002b. The glutamine commute: take the N line and transfer to the A. J. Cell Biol 157 (3), 349–355. [PubMed: 11980913]

Chowdhury GM, et al. 2007. Glutamatergic and GABAergic neurotransmitter cycling and energy metabolism in rat cerebral cortex during postnatal development. J. Cerebr. Blood Flow Metabol 27, 1895–1907.

Christensen HN, 1990. Role of amino acid transport and countertransport in nutrition and metabolism. Physiol. Rev 70 (1), 43–77. [PubMed: 2404290]

Clifford DB, et al. 1982. Effect of anticonvulsant drugs on kainic acid-induced epileptiform activity. Exp. Neurol 76, 156–167. [PubMed: 6806113]

Coleman N, et al. 2015. The riluzole derivative 2-amino-6-trifluoromethylthio-benzothiazole (SKA-19), a mixed KCa2 activator and NaV blocker, is a potent novel anticonvulsant. Neurotherapeutics 12, 234–249. [PubMed: 25256961]

Colovic M, Zennaro E, Caccia S, 2004. Liquid chromatographic assay for riluzole in mouse plasma and central nervous system tissues. J. Chromatogr 803, 305–309.

Conti F, Melone M, 2006. The glutamine commute: lost in the tube? Neurochem. Int 48 (6–7), 459–464. [PubMed: 16517023]

Danbolt NC, 2001. Glutamate uptake. Prog. Neurobiol 65 (1), 1–105. [PubMed: 11369436]

De Gois S, et al. 2005. Homeostatic scaling of vesicular glutamate and GABA transporter expression in rat neocortical circuits. J. Neurosci 25 (31), 7121–7133. [PubMed: 16079394]

Debono MW, et al. 1993. Inhibition by riluzole of electrophysiological responses mediated by rat kainate and NMDA receptors expressed in Xenopus oocytes. Eur. J. Pharmacol 235, 283–289. [PubMed: 7685290]

Deitmer JW, Broer A, Broer S, 2003. Glutamine efflux from astrocytes is mediated by multiple pathways. J. Neurochem 87 (1), 127–135. [PubMed: 12969260]

Deken SL, Wang D, Quick MW, 2003. Plasma membrane GABA transporters reside on distinct vesicles and undergo rapid regulated recycling. J. Neurosci 23, 1563–1568. [PubMed: 12629157]

Devinsky O, et al. 2018. Epilepsy. Nat. Rev. Dis. Primers 4. [PubMed: 29955060]

Doble A, 1996. The pharmacology and mechanism of action of riluzole. Neurology 47 (6 Suppl. 4), S233–S241. [PubMed: 8959995]

Dodd PR, 2002. Excited to death: different ways to lose your neurons. Biogerontology 3, 51–56. [PubMed: 12014842]

Dudek FE, Sutula TP, 2007. Epileptogenesis in the dentate gyrus: a critical perspective. Prog. Brain Res 163, 755–773. [PubMed: 17765749]

Dunleavy M, et al. 2010. Experimental neonatal status epilepticus and the development of temporal lobe epilepsy with unilateral hippocampal sclerosis. Am. J. Pathol 176, 330–342. [PubMed: 19948825]

Duprat F, et al. 2000. The neuroprotective agent riluzole activates the two P domain K( +) channels TREK-1 and TRAAK. Mol. Pharmacol 57, 906–912. [PubMed: 10779373]

Ebert U, Brandt C, Loscher W, 2002. Delayed sclerosis, neuroprotection, and limbic epileptogenesis after status epilepticus in the rat. Epilepsia. 10.1046/j.1528-1157.43.s.5.39.x.

Erickson JD, 2017. Functional identification of activity-regulated, high-affinity glutamine transport in hippocampal neurons inhibited by riluzole. J. Neurochem 142, 29–40. [PubMed: 28423185]

Errington AC, Stohr T, Lees G, 2005. Voltage gated ion channels: targets for anticonvulsant drugs. Curr. Top. Med. Chem 5, 15–30. [PubMed: 15638775]

Ferguson SM, et al. 2003. Vesicular localization and activity-dependent trafficking of presynaptic choline transporters. J. Neurosci 23, 9697–9709. [PubMed: 14585997]

Ferkany JW, Coyle JT, 1983. Kainic acid selectively stimulates the release of endogenous excitatory acidic amino acids. J. Pharmacol. Exp. Therapeut 225, 399–406.

Fisher PD, Sperber EF, Moshe SL, 1998. Hippocampal sclerosis revisited. Brain Dev. 20, 563–573. [PubMed: 9865538]

Fuller TA, Olney JW, 1981. Only certain anticonvulsants protect against kainate neurotoxicity. Neurobehav. Toxicol. Teratol 3, 355–361. [PubMed: 6793881]

Fumagalli E, et al. 2008. Riluzole enhances the activity of glutamate transporters GLAST, GLT1 and EAAC1. Eur. J. Pharmacol 578, 171–176. [PubMed: 18036519]

Gjessing LR, Gjesdahl P, Sjaastad O, 1972. The free amino acids in human cerebrospinal fluid. J. Neurochem 19 (7), 1807–1808. [PubMed: 5042475]

Grunnet M, et al. 2001. Pharmacological modulation of SK3 channels. Neuropharmacology 40, 879–887. [PubMed: 11378158]

Guerriero RM, Giza CC, Rotenberg A, 2015. Glutamate and GABA imbalance following traumatic brain injury. Curr. Neurol. Neurosci. Rep 10.1007/s11910-015-0545-1.

Haas KZ, et al. 2001. Resistance of immature hippocampus to morphologic and physiologic alterations following status epilepticus or kindling. Hippocampus 11, 615–625. [PubMed: 11811655]

Hanada T, 2020. Ionotropic glutamate receptors in epilepsy: a review focusing on AMPA and NMDA receptors. Biomolecules 10. 10.3390/biom10030464. [PubMed: 33374214]

Hassel B, Brathe A, 2000. Neuronal pyruvate carboxylation supports formation of transmitter glutamate. J. Neurosci 20, 1342–1347. [PubMed: 10662824]

Henze DA, Urban NN, Barrionuevo G, 2000. The multifarious hippocampal mossy fiber pathway: a review. Neuroscience 98, 407–427. [PubMed: 10869836]

Herbert T, et al. 1994. Block of the rat brain IIA sodium channel alpha subunit by the neuroprotective drug riluzole. Mol. Pharmacol 45, 1055–1060. [PubMed: 8190096]

Hertz L, 2013. The glutamate-glutamine (GABA) cycle: importance of late postnatal development and potential reciprocal interactions between biosynthesis and degradation. Front. Endocrinol 4, 1–16.

Holmes GL, 2002. Seizure-induced neuronal injury: animal data. Neurology 59, S3–S6.

Hopkins KJ, Wang G-J, Schmued LC, 2000. Temporal progression of kainic acid induced neuronal and myelin degeneration in the rat forebrain. Brain Res. 864, 69–80. [PubMed: 10793188]

Horton DA, Bourne GT, Smythe ML, 2003. The combinatorial synthesis of bicyclic privileged structures or privileged substructures. Chem. Rev 103, 893–930. [PubMed: 12630855]

Huang CS, et al. 1997. Effects of the neuroprotective agent riluzole on the high voltage-activated calcium channels of rat dorsal root ganglion neurons. J. Pharmacol. Exp. Therapeut 282, 1280–1290.

Jagbir G, et al. 2015. Anticonvulsant and neurological profile of benzothiazoles: a mini-review. Cent. Nerv. Syst. Agents Med. Chem 15, 11–16. [PubMed: 25578435]

Janszky J, et al. 2005. Temporal lobe epilepsy with hippocampal sclerosis: predictors for long-term surgical outcome. Brain 128, 395–404. [PubMed: 15634733]

Jimonet P, et al. 1994. Synthesis, anticonvulsant and neuroprotective activities of RP 66055, a riluzole derivative. Bioorg. Med. Chem 2, 793–798. [PubMed: 7894973]

Kam K, Nicoll R, 2007. Excitatory synaptic transmission persists independently of the glutamate-glutamine cycle. J. Neurosci 27 (34), 9192–9200. [PubMed: 17715355]

Kaminski RM, Rogawski MA, Klitgaard H, 2014. The potential of antiseizure drugs and agents that act on novel molecular targets as antiepileptogenic treatments. Neurotherapeutics 11, 385–400. [PubMed: 24671870]

Kanamori K, Ross BD, 2004. Quantitative determination of extracellular glutamine concentration in rat brain, and its elevation in vivo by system A transport inhibitor, alpha-(methylamino)isobutyrate. J. Neurochem 90 (1), 203–210. [PubMed: 15198679]

Kanamori K, Ross BD, 2011. Chronic electrographic seizure reduces glutamine and elevates glutamate in the extracellular fluid of rat brain. Brain Res. 1371, 180–191. [PubMed: 21111723]

Kanamori K, Ross BD, 2013. Electrographic seizures are significantly reduced by in vivo inhibition of neuronal uptake of extracellular glutamine in rat hippocampus. Epilepsy Res. 107, 20–36. [PubMed: 24070846]

Kim JE, et al. 2007. Anti-glutamatergic effect of riluzole: comparison with valproic acid. Neuroscience 147, 136–145. [PubMed: 17507170]

Kvamme E, Torgner IA, Roberg B, 2001. Kinetics and localization of brain phosphate activated glutaminase. J. Neurosci. Res 66 (5), 951–958. [PubMed: 11746423]

Leke R, Schousboe A, 2016. The glutamine transporters and their role in the glutamate/GABA-glutamine cycle. Adv. Neurobiol 13, 223–257. [PubMed: 27885631]

Levesque M.a.A.M., 2013. The kainic acid model of temporal lobe epilepsy. Neurosci Behav Rev 37, 2887–2899.

Lingamaneni R, Hemmings HC, 1999. Effects of anticonvulsants on veratridine- and KCl-evoked glutamate release from rat cortical synaptosomes. Neurosci. Lett 276, 127–130. [PubMed: 10624808]

Lipton SA, 2004. Failures and successes of NMDA receptor antagonists: molecular basis for the use of open-channel blockers like memantine in the treatment of acute and chronic neurologic insults. NeuroRx 1, 101–110. [PubMed: 15717010]

Loscher W, 2020. The holy grail of epilepsy prevention: preclinical approaches to antiepileptogenic treatments. Neuropharmacology 167, 107605. [PubMed: 30980836]

Loscher W, Klein P, 2021. The pharmacology and clinical efficacy of antiseizure medications: from bromide salts to cenobamate and beyond. CNS Drugs 35, 935–963. [PubMed: 34145528]

Loscher W, Schmidt D, 2011. Modern antiepileptic drug development has failed to deliver: ways out of the current dilemma. Epilepsia 52, 657–678. [PubMed: 21426333]

Loscher W, Schmidt D, 2012. Perampanel-new promise for refractory epilepsy? Nat. Rev. Neurol 8, 661–662. [PubMed: 23147851]

Loscher W, et al. 2020. Drug resistance in epilepsy: clinical impact, potential mechanisms, and new innovative treatment options. Pharmacol. Rev 72, 606–638. [PubMed: 32540959]

Mackenzie B, Erickson JD, 2004. Sodium-coupled neutral amino acid (System N/A) transporters of the SLC38 gene family. Pflügers Archiv 447 (5), 784–795. [PubMed: 12845534]

Mackenzie B, et al. 2003. Functional properties and cellular distribution of the system A glutamine transporter SNAT1 support specialized roles in central neurons. J. Biol. Chem 278 (26), 23720–23730. [PubMed: 12684517]

Marques FVBS, et al. 2022. Pharmacological perspectives and mechanisms involved in epileptogenesis. Beni-Suef Univ J Basic Appl. Sci 11. Article number: 97.

Martin D, Thompson MA, Nadler JD, 1993. The neuroprotective agent riluzole inhibits release of glutamate and aspartate from slices of hippocampal area CA1. Eur. J. Pharmacol 250, 473–476. [PubMed: 8112408]

Marx M-C, Billups D, Billups B, 2015. Maintaining the presynaptic glutamate supply for excitatory neurotransmission. J. Neurosci. Res 93, 1031–1044. [PubMed: 25648608]

Masson J, et al. 2006. Mice lacking brain/kidney phosphate-activated glutaminase have impaired glutamatergic synaptic transmission, altered breathing, disorganized goal-directed behavior and die shortly after birth. J. Neurosci 26, 4660–4671. [PubMed: 16641247]

Maycox PR, Hell JW, Jahn R, 1990. Amino acid neurotransmission: spotlight on synaptic vesicles. Trends Neurosci. 13, 83–87. [PubMed: 1691873]

McGale EH, et al. 1977. Studies of the inter-relationship between cerebrospinal fluid and plasma amino acid concentrations in normal individuals. J. Neurochem 29 (2), 291–297. [PubMed: 886334]

Meisler MH, Hill SF, Yu W, 2021. Sodium channelopathies in neurodevelopmental disorders. Nat. Rev. Neurosci 22, 152–166. [PubMed: 33531663]

Meldrum BS, Rogawski MA, 2007. Molecular targets for antiepileptic drug development. Neurotherapeutics 4, 18–61. [PubMed: 17199015]

Melone M, et al. 2004. Localization of the glutamine transporter SNAT1 in rat cerebral cortex and neighboring structures, with a note on its localization in human cortex. Cerebr. Cortex 14 (5), 562–574.

Melone M, et al. 2006. Localization of the Na(+)-coupled neutral amino acid transporter 2 in the cerebral cortex. Neuroscience 140 (1), 281–292. [PubMed: 16616430]

Mizoule J, et al. 1985. 2-amino-6-trifuoromethoxy benzothiazole, a possible antagonist of excitatory amino acid neurotransmission: I. Anti-convulsant properties. Neuropharmacology 24, 767–773. [PubMed: 3018617]

Moechars D, et al. 2006. Vesicular glutamate transporter VGLUT2 expression levels control quantal size and neuropathic pain. J. Neurosci 26 (46), 12055–12066. [PubMed: 17108179]

Muir KW, 2006. Glutamate-based therapeutic approaches: clinical trials with NMDA antagonists. Curr. Opin. Pharmacol 6, 53–60. [PubMed: 16359918]

Mukhtar I, 2020. Inflammatory and immune mechanisms underlying epileptogenesis and epilepsy: from pathogenesis to treatment target. Seizure 82, 65–79. [PubMed: 33011590]

Mullen RJ, Buck CR, Smith AM, 1992. NeuN, a Neuronal Specific Nuclear Protein in vertebrates, vol. 116. Development, pp. 201–211. [PubMed: 1483388]

Nadler JV, 1981. Role of excitatory pathways in the hippocampal damage produced by kainic acid. Adv. Biochem. Psychopharmacol 27, 395–402. [PubMed: 7004120]

Nitecka L, et al. 1984. Maturation of kainic acid seizure-brain damage syndrome in the rat. II. Histopathological sequelae. Neuroscience 13, 1073–1094. [PubMed: 6527790]

Noh KM, et al. 2000. A novel neuroprotective mechanism of riluzole: direct inhibition of protein kinase C. Neurobiol. Dis 7, 375–383. [PubMed: 10964608]

Norenberg MD, Martinez-Hernandez A, 1979. Fine structural localization of glutamine synthetase in astrocytes of rat brain. Brain Res. 161, 303–310. [PubMed: 31966]

O'Malley HA, Isom LL, 2016. Sodium channel B subunits: emerging targets in channelopathies. Annu. Rev. Physiol 77, 481–504.

Pal R, et al. 2021. Voltage gated sodium channel inhibitors as anticonvulsant drugs: a systematic review on recent developments and structure activity relationship studies. Bioorg. Chem 115 10.1016/j.bioorg.2021.105230.

Pelletier JC, et al. 2018. Dipeptide prodrugs of the glutamate modulator riluzole. ACS Med. Chem. Lett 9, 752–756. [PubMed: 30034613]

Perucca P, Gilliam FG, 2012. Adverse effects of antiepileptic drugs. Lancet Neurol. 11, 792–802. [PubMed: 22832500]

Perucca E, Meador KJ, 2005. Adverse effects of antiepileptic drugs. Acta Neurol. Scand. Suppl 181, 30–35. [PubMed: 16238706]

Pietrancosta N, et al. 2020. Molecular, structural, functional, and pharmacological sites for vesicular glutamate transporter regulation. Mol. Neurobiol 30, 1–25.

Pitkanen A, Sutula TP, 2002. Is epilepsy a progressive disorder? Prospects for new therapeutic approaches in temporal-lobe epilepsy. Lancet Neurol. 1, 173–181. [PubMed: 12849486]

Pont F, Collet A, Lallement G, 1995. Early and transient increase of rat hippocampal blood-brain barrier permeability to amino acids during kainic acid-induced seizures. Neurosci. Lett 184, 52–54. [PubMed: 7739806]

Prakriya M, Mennerick S, 2000. Selective depression of low-release probability excitatory synapses by sodium channel blockers. Neuron 26, 671–682. [PubMed: 10896162]

Priyanka SNK, Jha KK, 2010. Benzothiazole: the molecule of diverse biological activities. Int. J. Curr. Pharmaceut. Res 2, 1–6.

Racine RJ, 1972. Modification of seizure activity by electrical stimulation. II. Motor seizure. Neurophysiology 32, 281–294.

Reimer RJ, et al. 2000. Amino acid transport system A resembles system N in sequence but differs in mechanism. Proc. Natl. Acad. Sci. U. S. A 97 (14), 7715–7720. [PubMed: 10859363]

Riban V, et al. 2002. Evolution of hippocampal epileptic activity during the development of hippocampal sclerosis in a mouse model of temporal lobe epilepsy. Neuroscience 112, 101–111. [PubMed: 12044475]

Rizk ML, et al. 2017. Importance of drug pharmacokinetics at the site of action. Clin. Transl. Sci 10, 133–142. [PubMed: 28160433]

Rodriguez RA, et al. 2014. Palau'chlor: a practical and reactive chlorinating reagent. J. Am. Chem. Soc 136, 6908–6911. [PubMed: 24758725]

Rogawski MA, 2013. AMPA receptors as a molecular target in epilepsy therapy. Acta Neurol. Scand. Suppl, 9–18. [PubMed: 23480151]

Romettino S, Lazdunski M, Gottesmann C, 1991. Anticonvulsant and sleep-waking influences of riluzole in a rat model of absence epilepsy. Eur. J. Pharmacol 199, 371–373. [PubMed: 1915583]

Rosker C, et al. 2007. The TTX metabolite 4,9-andydro-TTX is a highly specific blocker of the Na-v1.6 voltage-dependent sodium channel. Am. J. Physiol. Cell Physiol 293, C783–C789. [PubMed: 17522141]

Rothstein JD, et al. 1996. Knockout of glutamate transporters reveals a major role for astroglial transport in excitotoxicity and clearance of glutamate. Neuron 16, 675–686. [PubMed: 8785064]

Rusina E, Bernard C, Williamson A, 2021. The kainic acid models of temporal lobe epilepsy. eNeuro 8.

Saito K, et al. 2010. The physiological roles of vesicular GABA transporter during embryonic development: a study using knockout mice. Mol. Brain 3. 10.1186/1756-6606-3-40. [PubMed: 20205763]

Salameh JS, Brown RH, Berry JD, 2015. Amyotrophic lateral sclerosis: review. Semin. Neurol 35, 469–476. [PubMed: 26502769]

Saletti PG, et al. 2019. In search of antiepileptogenic treatments for post-traumatic epilepsy. Neurobiol. Dis 123, 86–99. [PubMed: 29936231]

Sankaranarayanan A, et al. 2009. Naphtho[1,2-d]thiazol-2-ylamine (SLA-31, a new activator of KCa2 and KCa3.1 potassium channels), potentiates the endothelium-derived hyperpolarizing factor response and lowers blood pressure. Mol. Pharmacol 75, 281–295. [PubMed: 18955585]

Schidlitzki A, et al. 2017. A combination of NMDA and AMPA receptor antagonists retards granule cell dispersion and epileptogenesis in a model of acquired epilepsy. Sci. Rep 10.1038/s41598-017-12368-6.

Schmued LC, Hopkins KJ, 2000. Fluoro-Jade B: a high affinity fluorescent marker for the localization of neuronal degeneration. Brain Res. 874, 123–130. [PubMed: 10960596]

Schousboe A, et al. 1997. Trafficking between glia and neurons of TCA cycle intermediates and related metabolites. Glia 21, 99–105. [PubMed: 9298852]

Sharma AK, et al. 2007. Mesial temporal lobe epilepsy: pathogenesis, induced rodent models and lesions. Toxicol. Pathol 35, 984–999. [PubMed: 18098044]

Sharma PC, et al. 2012. Medicinal significance of benzothiazole scaffold: an insight view. J. Enzym. Inhib. Med. Chem 28 (2), 240–266.

Sheldon AL, Robinson MB, 2007. The role of glutamate transporters in neurodegenerative diseases and potential opportunities for intervention. Neurochem. Int 51, 333–355. [PubMed: 17517448]

Shim H, et al. 2019. The trials and tribulations of structure assisted design of KCa Channel activators. Front. Pharmacol doi.org/. 10.3389/fphar.2019.00972.

Sills GJ, Rogawski MA, 2020. Mechanisms of action of currently used antiseizure drugs. Neuropharmacology 168, 107966. [PubMed: 32120063]

Sirven JI, 2015. Epilepsy: a spectrum disorder. Cold Spring Harb. Perspect Med 5, a022848. [PubMed: 26328931]

Song JH, et al. 1997. Differential action of riluzole on tetrodotoxin-sensitive and tetrodotoxin-resistant sodium channels. J. Pharmacol. Exp. Therapeut 282, 707–714.

Spadoni F, et al. 2002. Lamotrigine derivatives and riluzole inhibit INa2P in cortical neurons. Neuroreport 13, 1167–1170. [PubMed: 12151762]

Sperk G, 1994. Kainic acid seizures in the rat. Prog. Neurobiol 42, 1–32. [PubMed: 7480784]

Srivastava A, et al. 2020. Quantitative Neurotoxicology: an assessment of the neurotoxic profile of kainic acid in Sprague Dawley rats. Int. J. Toxicol 39, 294–306. [PubMed: 32468881]

Stefani A, Spadoni F, Bernardi G, 1997. Differential inhibition by riluzole, lamotrigine, and phenytoin of sodium and calcium currents in cortical neurons: implications for neuroprotective strategies. Exp. Neurol 147, 115–122. [PubMed: 9294408]

Stepan AF, et al. 2011. Structural alert/reactive metabolite concept as applied in medicinal chamistry to mitigate the risk of idiosyncratic drug toxicity; a perspective based on the critical examination of trends in the top 200 drugs marketed in the United States. Chem. Res. Toxicol 24, 1345–1410. [PubMed: 21702456]

Stutzmann JM, et al. 1997. Neuroprotective profile of riluzole in in vivo models of acute neurodegenerative diseases. CNS Drug Rev. 3, 83–101.

Sudhof TC, 2012. Calcium control of neurotransmitter release. Cold Spring Harbor Perspect. Biol 41 10.1101/cshperspect.a011353.

Takamori S, et al. 2000. Identification of a vesicular glutamate transporter that defines a glutamatergic phenotype in neurons. Nature 407 (6801), 189–194. [PubMed: 11001057]

Takeda K, et al. 2012. Synaptic vesicles are capable of synthesizing the VGLUT substrate glutamate from α-ketoglutarate for vesicular loading. J. Neurochem 121, 184–196. [PubMed: 22309504]

Tang F, Hartz AMS, Bauer B, 2017. Drug-resistant epilepsy: multiple hypotheses, few answers. Front. Neurol, 10.3389/fneur.2017.0030.

Tani H, et al. 2007. Modulation of epileptiform activity by glutamine and system A transport in a model of post-traumatic epilepsy. Neurobiol. Dis 25 (2), 230–238. [PubMed: 17070687]

Tani H, et al. 2010. Glutamine is required for persistent epileptiform activity in the disinhibited neocortical brain slice. J. Neurosci 30, 1288–1300. [PubMed: 20107056]

Tani H, et al. 2014. A local glutamate-glutamine cycle sustains synaptic excitatory transmitter release. Neuron 81, 888–900. [PubMed: 24559677]

Teramoto N, Yotsu-Yamashita M, 2015. Selective blocking effects of 4,9-anhydrotetrodotoxin, purified from a crude mixture of tetrodotoxin analogues, on NaV1.6 channels and its chemical aspects. Mar. Drugs 13, 984–995. [PubMed: 25686275]

Thigpen J, Miller SE, Pond BB, 2013. Behavioral side effects of antiepileptic drugs. U.S. Pharm 38, HS15–HS20.

Thom M, 2014. Review: hippocampal sclerosis in epilepsy: a neuropathology review. Neuropathol. Appl. Neurobiol 40, 520–543. [PubMed: 24762203]

Treyer A, et al. 2018. Intracellular drug bioavailability: effect of neutral lipids and phospholipids. Mol. Pharm 15, 2224–2233. [PubMed: 29709195]

Ugale VG, et al. 2012. Quinazolino-benzothiazoles: fused pharmacophores as anticonvulsant agents. Eur. J. Med. Chem 53, 107–113. [PubMed: 22534186]

Varoqui H, et al. 2000. Cloning and functional identification of a neuronal glutamine transporter. J. Biol. Chem 275 (6), 4049–4054. [PubMed: 10660562]

Verma SK, et al. 2016. Enhancement in the neuroprotective power of riluzole against cerebral ischemia using a brain targeted drug delivery vehicle. ACS Appl. Mater. Interfaces 8, 19716–19723. [PubMed: 27378322]

Vezzani A, et al. 2011. The role of inflammation in epilepsy. Nat. Rev. Neurol 7, 31–40. [PubMed: 21135885]

Vezzani A, Balosso S, Ravizza T, 2019. Neuroinflammatory pathways as treatment targets and biomarkers in epilepsy. Nat. Rev. Neurol 15, 459–472. [PubMed: 31263255]

Walia KS, et al. 2004. Side effects of anti epileptics - a review. Pain Pract. 4, 194–203. [PubMed: 17173601]

Wang SJ, Wang KY, Wang WC, 2004. Mechanisms underlying the riluzole inhibition of glutamate release from rat cerebral cortex nerve terminals (synaptosomes). Neuroscience 125, 191–201. [PubMed: 15051158]

Wang Q, et al. 2005. Kainic acid-mediated excitotoxieity as a model for neurodegeneration. Mol. Neurobiol 31, 3–16. [PubMed: 15953808]

Wasling P, Hanse E, Gustafsson B, 2004. Developmental changes in release properties of the CA3-CA1 glutamate synapse in rat hippocampus. J. Neurophysiol 92 (5), 2714–2724. [PubMed: 15295011]

Watson C, 2003. Hippocampal sclerosis and the syndrome of medial temporal lobe epilepsy. Expert Rev. Neurother 3, 821–828. [PubMed: 19810885]

Weiss MD, et al. 2003. Ontogeny of the neutral amino acid transporter SAT1/ATA1 in rat brain. Brain Res Dev Brain Res 143, 151–159. [PubMed: 12855186]

White HS, Bialer M, 2010. Key factors in the discovery and development of new antiepileptic drugs. Nat. Rev. Drug Discov 9, 68–82. [PubMed: 20043029]

Wilson N, Kang J, Hueske E, Leung T, Varoqui H, Murnick J, Erickson J, Liu G, 2005. Presynaptic regulation of quanta! size by the vesicular glutamate transporter (VGLUT1). J. Neurosci 25, 6221–6234. [PubMed: 15987952]

Wozniak DF, et al. 1991. Age-related sensitivity to kainate neurotoxicity. Exp. Neurol 114, 250–253. [PubMed: 1748199]

Yao D, et al. 2000. A novel system A isoform mediating Na+/neutral amino acid cotransport. J. Biol. Chem 275 (30), 22790–22797. [PubMed: 10811809]

Zona C, et al. 1998. Riluzole interacts with voltage-activated sodium and potassium currents in cultured rat cortical neurons. Neuroscience 85, 931–938. [PubMed: 9639285]

Zona C, et al. 2002. Kainate-induced currents in rat cortical neurons in culture are modulated by riluzole. Synapse 43, 244–251. [PubMed: 11835519]

Zucker DK, Wooten GF, Lothman EW, 1983. Blood-brain barrier changes with kainic acid-induced limbic seizures. Exp. Neurol 79, 422–433. [PubMed: 6822273]

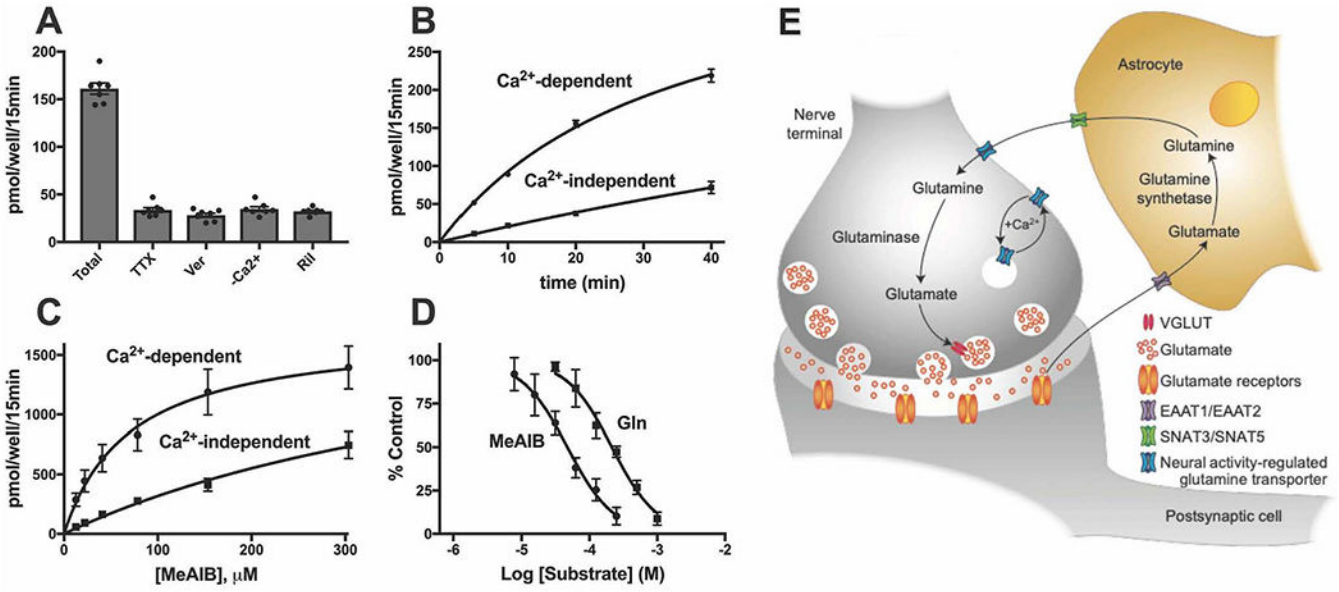


**Fig. 1.**

Spontaneous high affinity MeAIB/Gln transport activity is regulated by neural activity in mature (DIV 19–21) neuron-enriched rat hippocampal networks *in vitro*. A, $^{14}$C-MeAIB transport (5.4 μM) is inhibited by tetrodotoxin (TTX; 1 μM), verapamil (Ver; 25 μM), omission of $Ca^{2+}$ ion, or by riluzole (Ril; 10 μM). Transport experiments were conducted over a 15 min period and background levels determined at 4 °C were subtracted. **B,** Time-courses of $Ca^{2+}$-dependent and $Ca^{2+}$-independent $^{14}$C-MeAIB uptake. $Ca^{2+}$-dependent values are total $^{14}$C-MeAIB (5.4 μM) uptake minus uptake in the absence of $Ca^{2+}$. $Ca^{2+}$ independent values have 4 °C values subtracted. **C,** Michaelis-Menten kinetic analysis of $Ca^{2+}$-dependent and $Ca^{2+}$-independent transport activity reveal high and low affinity systems. Background values (−$Ca^{2+}$ or 4 °C) at each MeAIB concentration were subtracted. **D,** The relative high affinity of Gln for spontaneous $Ca^{2+}$-dependent transport was determined by competition analysis ($IC_{50}$) with $^{14}$C-MeAIB (5.4 μM). Background is uptake in absence of $Ca^{2+}$ and was subtracted from all values. All final determinations above were from 3 to 5 independent neuronal cultures and are presented as mean values±SEM with critical significance level of $p < 0.05$. **E,** Model of the Glu/Gln cycle between neurons and astrocytes that recycles Glu for neurotransmission indicates where the neuronal activity regulated MeAIB/Gln transport system that we describe here (*blue transporter*) may support the concept of a $Ca^{2+}$-dependent pathway for cycling of this high affinity transporter by neural activity in synaptic terminals (modified from (Erickson, 2017)).

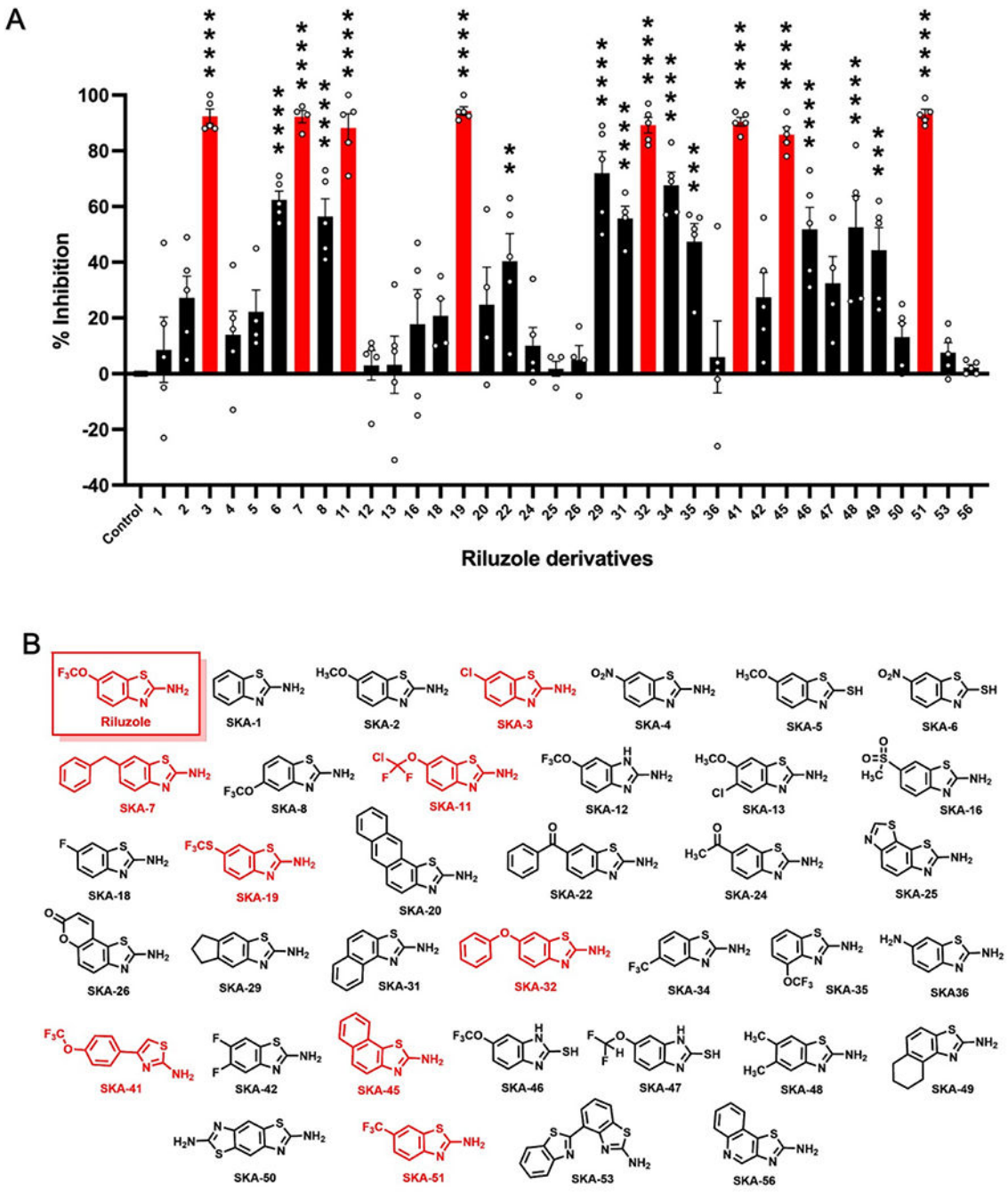


**Fig. 2.**

SKA-41 is an aminothiazole derivative of riluzole that inhibits spontaneous, neural activity regulated and high affinity MeAIB/Gln transport. A, We used a library of riluzole derivatives to screen in a first round for compounds that retain the ability to inhibit neural activity regulated high affinity MeAIB/Gln transport, yet may be structurally unique. All compounds (20 μM) were added together with $^{14}$C-MeAIB (23.4 μM). Most active structures presented are conventional benzothiazoles derived from riluzole. However, SKA-41 is structurally distinguished being an “open” 4-phenyl-aminothiazole. **B,** $^{14}$C-MeAIB transport is presented

as a % of control neural activity regulated values. *Red* highlights reveal the active compounds in this first screen (n = 3 ± SEM). All values are results from independent neuronal cultures with critical significance level of $p < 0.05$.

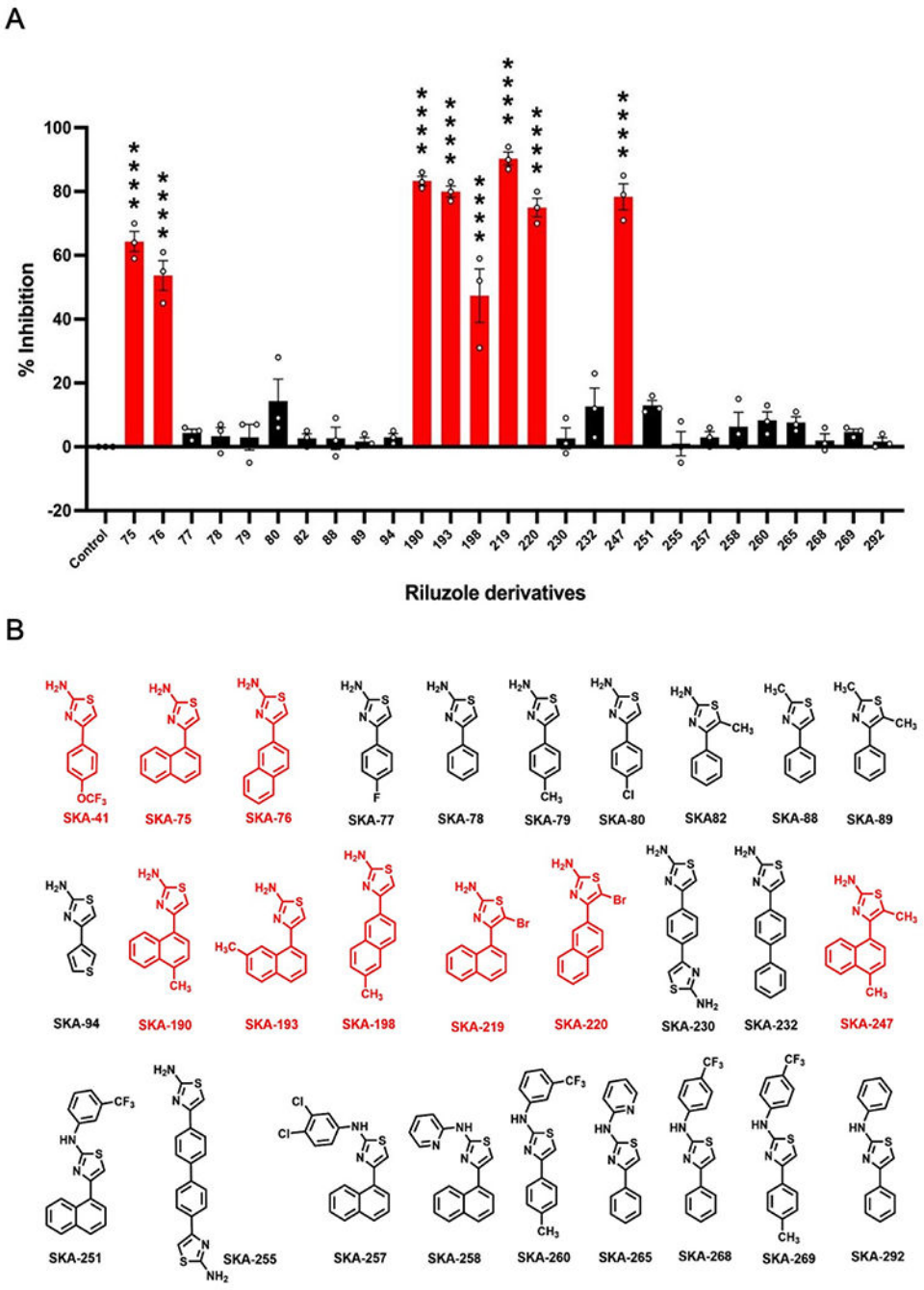


**Fig. 3.**

Screening of SKA-41 related compounds that inhibit spontaneous, activity regulated MeAIB/Gln transport reveals common structures. A, SKA-41 and related 4-phenyl- and naphthalenyl substituted aminothiazoles were screened in a 2nd round to evaluate their relative inhibitory potency at 10 μM concentration to inhibit $^{14}$C-MeAIB (5.4 μM) uptake and identify compounds that retain the ability to inhibit high affinity MeAIB/Gln transport like SKA-41, and are structurally related. Active compounds are mostly derived from SKA-75 (SKA-190, SKA-193, SKA-219, SKA-247) or from the regioisomer SKA-76

(SKA-198, SKA-220). SKA-219 is the most potent inhibitor evaluated in this 2nd screen. **B**, $^{14}$C-MeAIB transport is presented as a % of control neural activity regulated values. *Red* highlights reveal the active compounds in this second screen (n = 3 ± SEM). All values are results from independent neuronal cultures with critical significance level of $p < 0.05$.

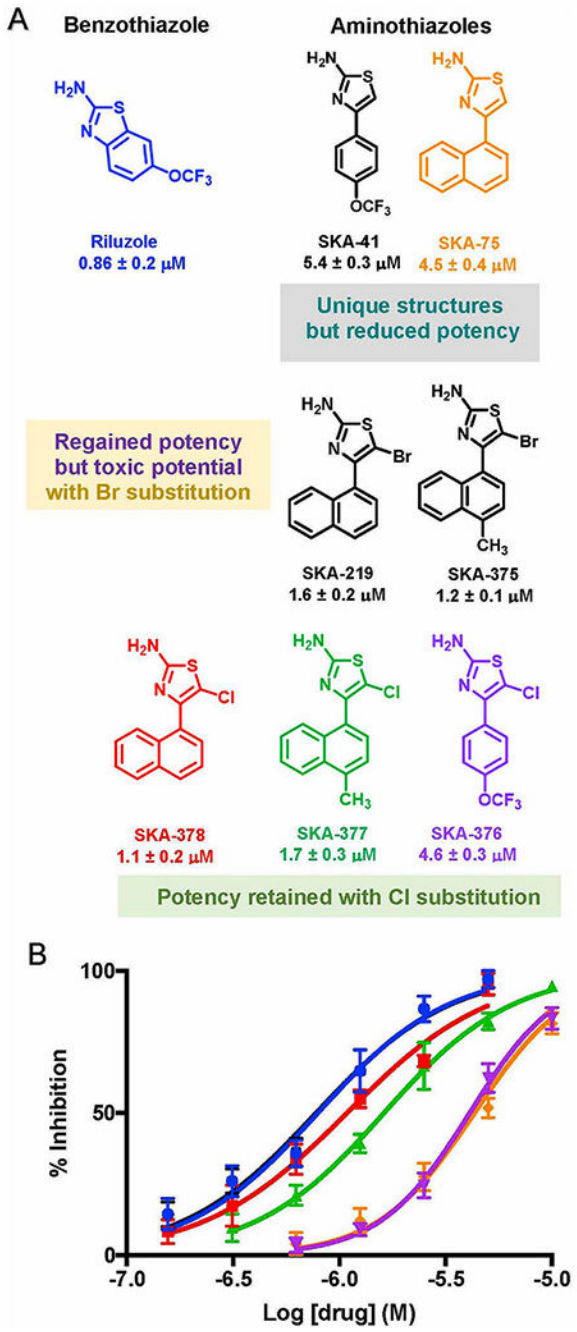


**Fig. 4.**

Novel chlorinated aminothiazole entities derived from SKA-75 inhibit spontaneous, activity-regulated and high-affinity MeAIB/Gln transport. A, Screening strategy: Screen 1 of riluzole derivatives identified SKA-41 as an active aminothiazole compound. Screen 2 identified SKA-75 as an aminothiazole compound related to SKA-41 and was used for synthesis of most active agents described *in vitro* and *in vivo* here. **B,** Concentration response curves reveal that SKA-378 (*red*) and SKA-377 (*green*) similarly inhibit spontaneous, high affinity $^{14}$C-MeAIB transport activity like riluzole (*blue*). The curves are shifted to the right for

SKA-376 (*purple*), which is indistinguishable from SKA-75 (*orange*); yet all are still in the low micromolar range, n = 3–5 ± SEM. All values are results from independent neuronal cultures with critical significance level of $p < 0.05$.

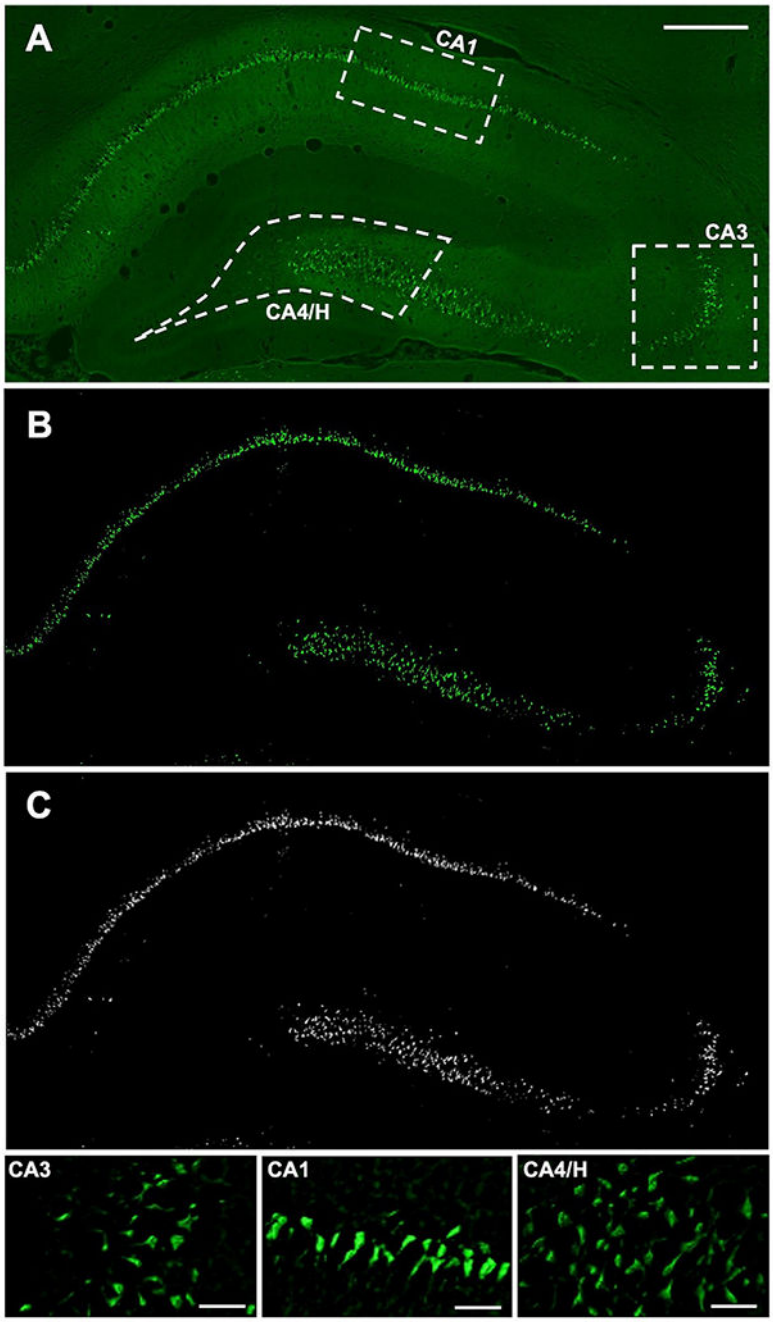


**Fig. 5.**

KA-induced SE results in acute hippocampal neural injury at 3 d. A. Respective images of FJB labeling in neuronal cell bodies and processes in the rat hippocampus following KA-induced SE. Boxes correspond to the areas of quantification for all rats. Scale bar = 400 μM. **B.** Same image as above but background fluorescence and staining in processes was subtracted. **C.** Green color channel was converted to white for quantification. **D.** High power (40x) images for CA3, CA1 and CA4/hilar region. Scale bar = 40 μm.

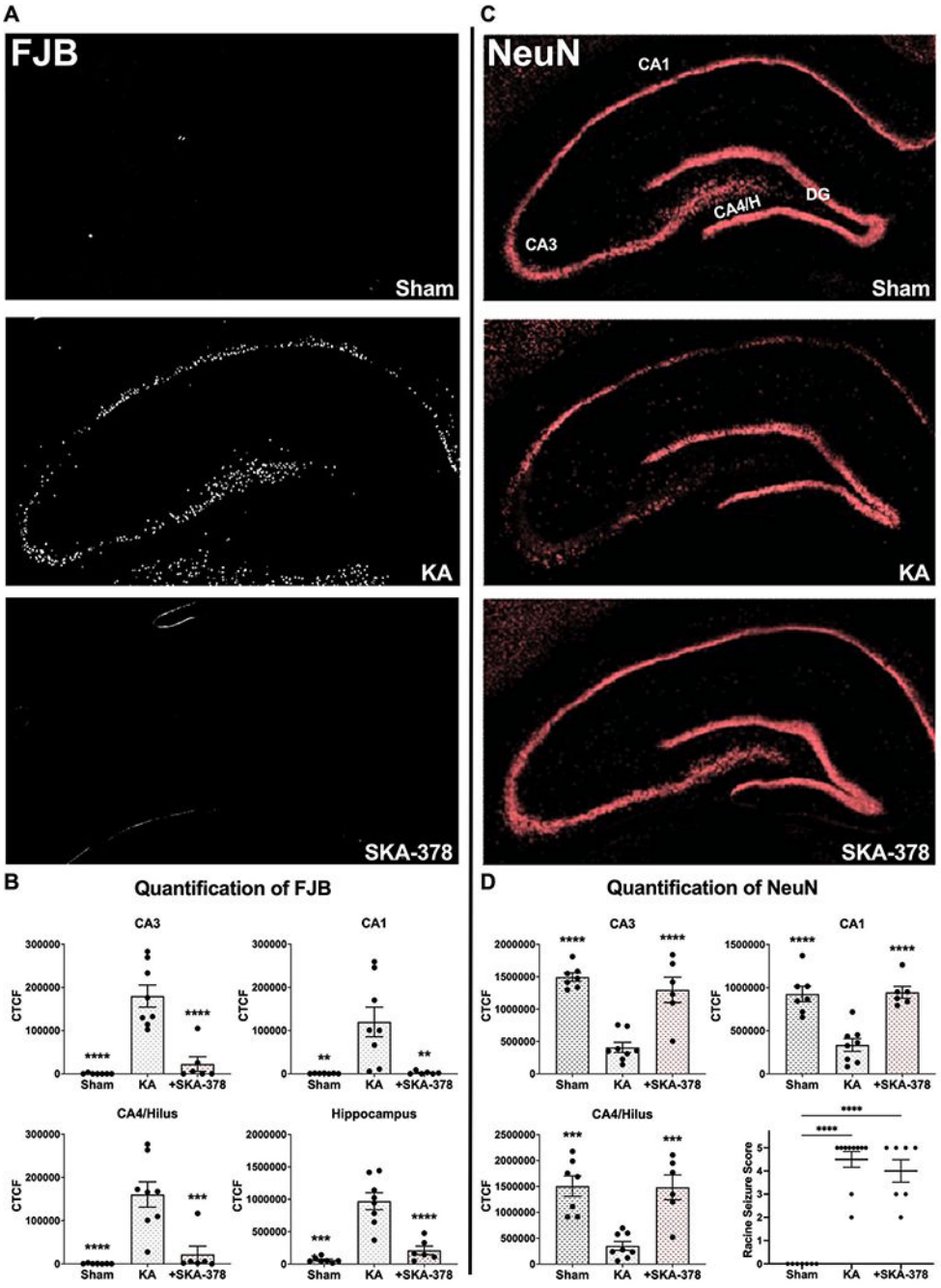


**Fig. 6.**

SKA-378 prevents acute hippocampal injury in the KA model of TLE. FJB and NeuN labeling was measured in sham (n = 7), KA treated rats (n = 8), and KA treated rats (n = 6) that were given SKA-378 (30 mg/kg, *i.p.*) 30 min prior KA injections., **A**, Representative examples of FJB labeling are shown as black and white images. Treatment of rats with SKA-378 largely prevents FJB labeling in the hippocampus. **B**, Quantification of the FJB results reveal that fluorescence intensity in KA-treated rats pretreated with SKA-378 was minimal in most hippocampal subfields and in the entire hippocampus. **C**, NeuN

immunostaining fluorescence was also measured in sham, KA treated rats, and KA treated rats pretreated with SKA-378. **D**. Quantification of the NeuN immunofluorescence intensity reveal that SKA-378 is neuroprotective in the CA1, CA3 and CA4 hippocampal subfields, n = 6–8 ± SEM. Repeated measures analysis of variance (ANOVA) followed by Dunnett's procedures to correct for multiple comparisons were used to analyze the results. A value of $p < 0.05$ is regarded as statistically significantly different than values from KA-treated rats, with asterisks corresponding to different levels of significance (**$p < 0.01$, ***$p < 0.001$, ****$p < 0.0001$).

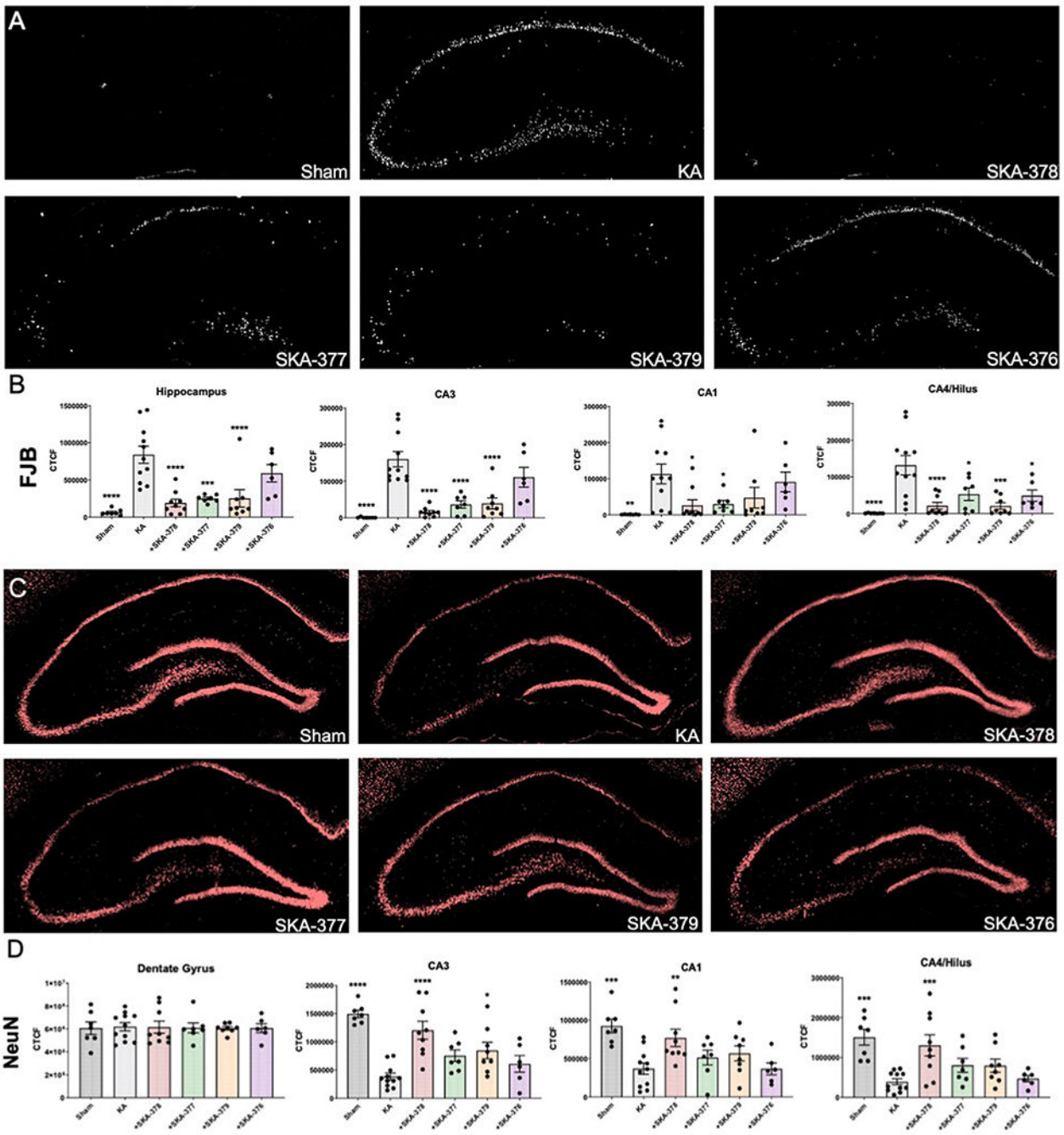


**Fig. 7.**

SKA-378 prevents neural injury when administered at 30 mg/kg after KA-induced status epilepticus (SE). Rats were treated with KA (5 mg/kg/h) until SE was observed and then 1 h after animals exhibited the first SE event they were injected with SKA-378 (n = 9), SKA-377 (n = 7), SKA-379 (n = 8), or SKA-376 (n = 6) at 30 mg/kg and then again 4 h after SE initiation followed by i.p. injections once/day for the next 2 d. Image analysis was conducted at 3 d. **A**, Representative examples of FJB labeling are shown as black and white images. Post-treatment of rats with SKA-378 largely prevents FJB labeling in the

hippocampus. **B**. Quantification of FJB staining in the entire hippocampus, and in the CA3, CA1 and CA4/Hilus subfields are presented. **C**. Representative examples of NeuN labeling. D. Quantification of NeuN immunofluorescence in the DG, and in the CA3, CA1 and CA4/Hilus subfields are shown. A value of $p < 0.05$ is regarded as statistically significantly different than values from KA-treated rats, with asterisks corresponding to different levels of significance (**$p < 0.01$, ***$p < 0.001$, ****$p < 0.0001$).

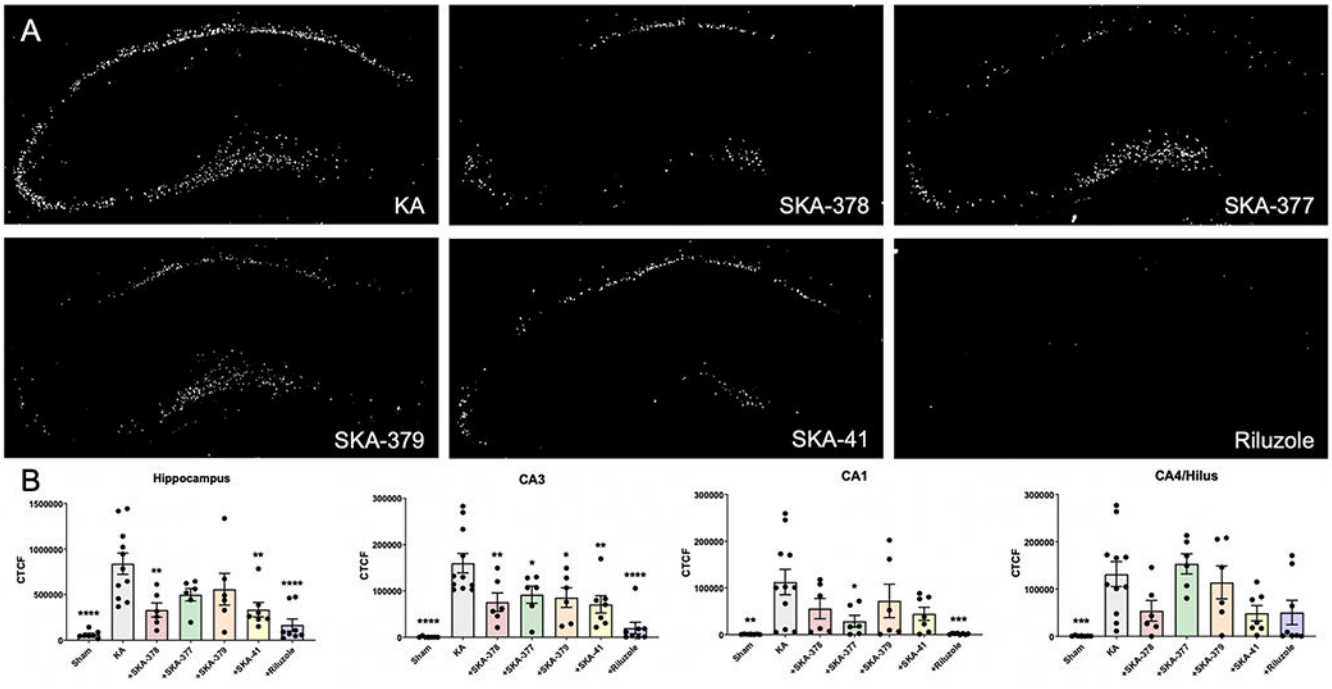


**Fig. 8.**

Riluzole prevents and SKA-378 attenuates neural injury when administered at 10 mg/kg after KA-induced status epilepticus (SE). Rats were treated with KA (5 mg/kg/h) until SE was observed and then 1 h after animals exhibited the first SE event they were injected with SKA-378 (n = 6), SKA-377 (n = 6), SKA-379 (n = 6), SKA-41 (n = 7) or riluzole (n = 8) at 10 mg/kg and then again 4 h after SE followed by i.p. injections once/day for the next 2 d. Image analysis was conducted at 3 d. **A**, Representative examples are shown as black and white images. **B**. Quantification of FJB staining in the entire hippocampus, and in the CA3, CA1 and CA4/Hilus subfields are presented. A value of $p < 0.05$ is regarded as statistically significantly different than values from KA-treated rats, with asterisks corresponding to different levels of significance (**$p < 0.01$, ***$p < 0.001$, ****$p < 0.0001$).

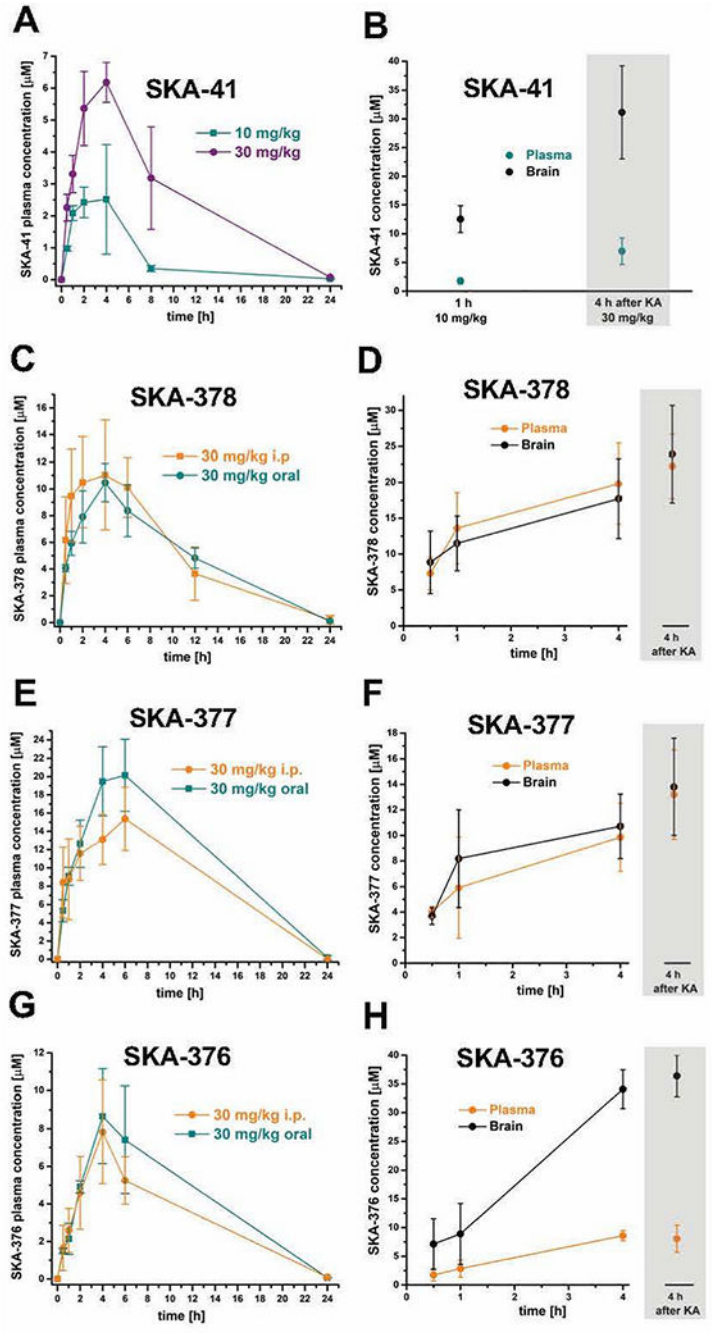


**Fig. 9.**

Plasma time-course and brain/plasma levels of SKA-41, SKA-376, SKA-377, SKA-378 and SKA-379. Effect of KA-induced SE. A, Total plasma concentrations of SKA-41 following oral administration at 10 and 30 mg/kg. **B,** Matched brain and plasma concentrations of SKA-41 at 1 h after i.p. administration of 10 mg/kg and at 4 h after i.p. administration of 30 mg/kg after KA. **C, E** and **G,** Total plasma concentrations of SKA-378, SKA-377 and SKA-376 following oral and i.p. administration at 30 mg/kg. **D, E** and **F,** Matched brain and plasma concentrations at 30 min, 1 h and 4 h after i.p. administration of SKA-378, SKA-377

and SKA-376 at 30 mg/kg. The grey shaded points show brain and plasma levels 5 h after KA administration. All data are total concentrations ± SD, n = 3 rats *per* time point.

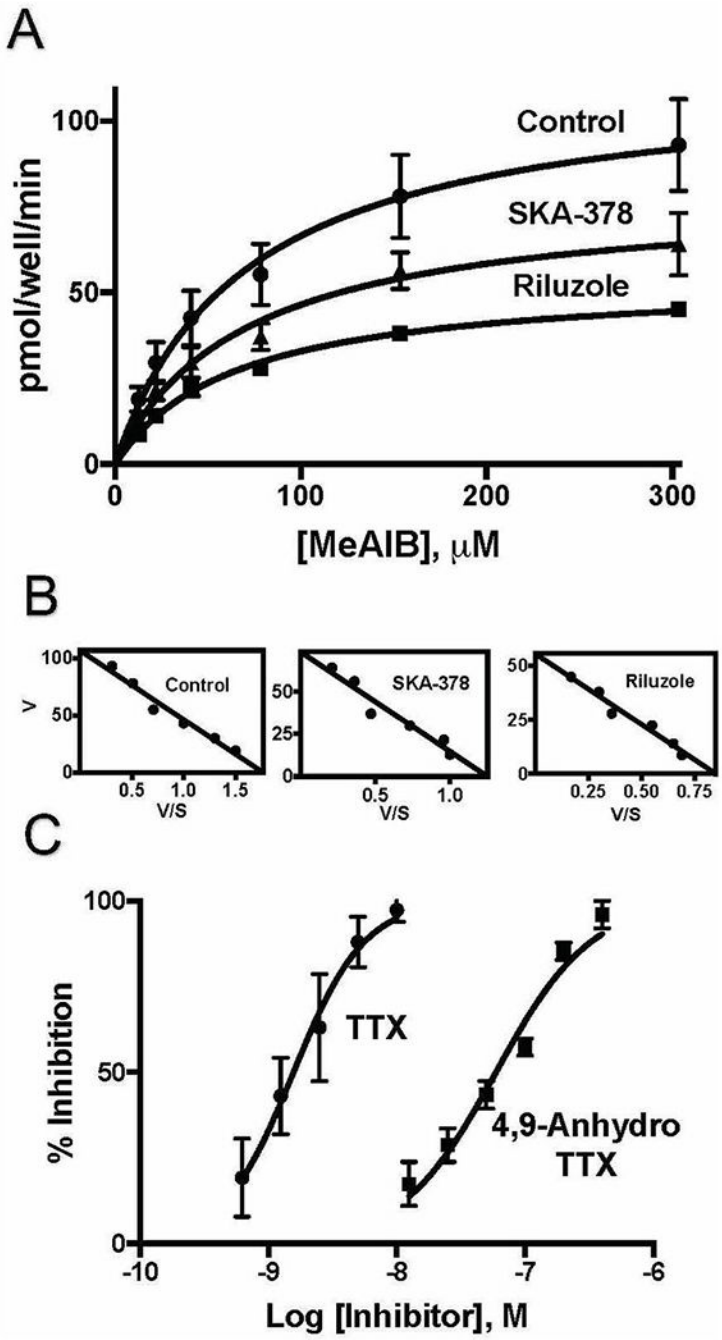


**Fig. 10.**

Non-competitive inhibition by riluzole and SKA-378 of spontaneous, neural activity regulated high affinity MeAIB/Gln transport activity in mature hippocampal neurons *in vitro.* A, Michaelis-Menten kinetic analysis of MeAIB uptake in the presence of riluzole or SKA-378 (1 μM). Background uptake was measured in the absence of $Ca^{2+}$ ion at each MeAIB concentration and was subtracted. **B,** Eadie-Hofstee scatchard analysis shows that the affinity of MeAIB ($K_m$, -slope) is not affected by riluzole or SKA-378 while the initial velocity (V, $V_{max}$) of transport is reduced by ~50% by both riluzole and SKA-378.

**C,** Inhibition of transport by the selective $Na_V1.6$ inhibitor 4,9-anhydroTTX. Background uptake was measured in the presence of 1 μM TTX and was subtracted. All values are results from independent neuronal cultures with critical significance level of $p < 0.05$.

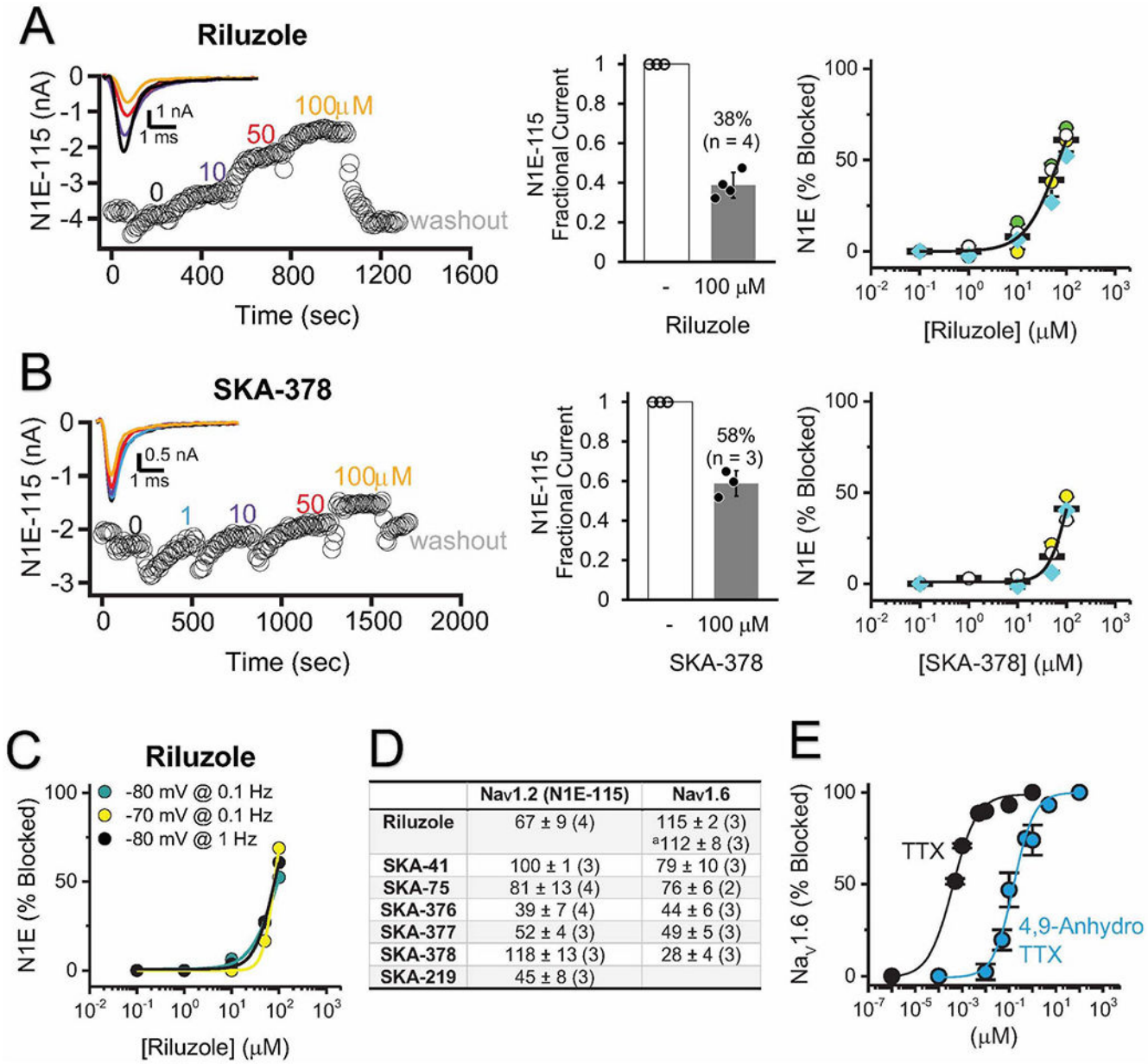


| | Nav1.2 (N1E-115) | Nav1.6 |
|---|---|---|
| **Riluzole** | 67 ± 9 (4) | 115 ± 2 (3)<br>[a]112 ± 8 (3) |
| **SKA-41** | 100 ± 1 (3) | 79 ± 10 (3) |
| **SKA-75** | 81 ± 13 (4) | 76 ± 6 (2) |
| **SKA-376** | 39 ± 7 (4) | 44 ± 6 (3) |
| **SKA-377** | 52 ± 4 (3) | 49 ± 5 (3) |
| **SKA-378** | 118 ± 13 (3) | 28 ± 4 (3) |
| **SKA-219** | 45 ± 8 (3) | |

**Fig. 11.**

Inhibition of $Na_V1.2$ and $Na_V1.6$ by riluzole, SKA-41, SKA-75, SKA-376, SKA-377, SKA-378 and SKA-219 determined by whole-cell patch-clamp. A, Effect of riluzole on native $Na_V1.2$ currents in N1E-115 cells. *Left*, Time course of current inhibition by increasing concentrations. *Middle*, Fractional block of 100 μM. *Right*, Concentration response curve. **B**, Effect of SKA-378 on native $Na_V1.2$ channels in N1E-115 cells. *Left*, Time course of current inhibition by increasing concentrations. *Middle*, Fractional block of 100 μM. *Right*, Concentration response curve. **C**, Inhibition of $Na_V1.2$ current by riluzole does not depend on holding potential or pulse frequency. **D**, Table showing IC**50** values ( ± SEM) in μM for $Na_V1.2$ and $Na_V1.6$ (holding potential −80 mV, inter-pulse interval 10 s (0.1 Hz). [a]recorded at 1 Hz to determine if there is any frequency dependence for riluzole on

$Na_V1.6$. **E**, Concentration response curves for TTX (n = 2) and 4,9-anhydroTTX on $Na_V1.6$. All values are results from data of 3 or 4 independent cells with critical significance level of $p < 0.05$.

## Table 1

$IC_{50}$ values of all active compounds tested for inhibition of spontaneous MeAIB transport activity, logP and % plasma protein binding.

| Compounds | $Ca^{2+}$-regulated MeAIB transport | logP | % plasma protein binding |
|---|---|---|---|
| Riluzole | 0.86 ± 0.02 (5) (μM) | 3.95 | 98 ± 0.5 |
| SKA-41 | 5.4 ± 0.2 (4) | 4.58 | 95.7 ± 0.4 |
| SKA-219 | 1.6 ± 0.23 (4) | 4.76 | 99.5 |
| SKA-378 | 1.1 ± 0.17 (4) | 4.2 | 99.2 ± 0.6 |
| SKA-75 | 4.5 ± 0.45 (4) | 4.05 | ND |
| SKA-190 | 2.6 ± 0.2 (4) | 4.53 | ND |
| SKA-376 | 4.3 ± 0.4 (4) | 4.53 | 98.5 ± 0.5 |
| SKA-377 | 1.7 ± 0.26 (4) | 4.91 | 99 ± 0.7 |
| SKA-379 | 6.5 ± 0.25 (5) | 4.42 | ND |
| SKA-382 | 12.2 ± 1.7 (4) | 4.14 | ND |
| SKA-76 | 6.2 ± 0.9 (5) | 4.05 | ND |
| SKA-220 | 4.3 ± 0.4 (5) | 4.42 | ND |
| SKA-375 | 1.2 ± 0.1 (3) | 5.25 | ND |
| TTX | 1.7 ± 0.2 nM (5) | – | – |
| 4,9-anhydroTTX | 61 ± 4 nM (3) | – | – |